Energy Reports 13 (2025) 1780–1801

Contents lists available at ScienceDirect

Energy Reports

journal homepage: www.elsevier.com/locate/egyr

Research paper

Enhancing vibration attenuation in offshore wind turbine with multiphysics mechanical metamaterial

M.R. Machado [a,b,*], M. Dutkiewicz [b]

[a] Faculty of Civil, Environmental Engineering and Architecture, Bydgoszcz University of Science and Technology, Al. Prof. Sylwestra Kaliskiego 7, Bydgoszcz, Poland
[b] Department of Mechanical Engineering, University of Brasilia, 70910-900, Brasília, Brazil

ARTICLE INFO

Keywords:
Tuned liquid damper
NREL 5MW monopile turbine
Spectral element method
Wind load
JONSWAP wave spectrum
Aerodynamic loads of blades

ABSTRACT

Wind energy harvesting is performed by wind turbines that convert wind into energy, contributing significantly to the increase in renewable energy globally. However, they encounter significant issues with structural vibrations caused by the operational environment, such as wind, wave, and seismic activities, which lead to malfunction, fatigue, and decreased efficiency. This paper proposes innovative metamaterial wind turbine designs that enhance vibration attenuation in offshore wind turbines by incorporating tuned liquid and multiphysics resonators. The locally resonant control mechanism improves the damping in the system by reducing displacement amplitude. These control strategies are tested under hazards, including wind, wave, and blade rotation, and evaluate various liquid configurations to determine optimal performance. The findings show a substantial reduction in overall vibration amplitude, achieving up to 60% of vibration amplitude attenuation, compared to 7.8% with traditional tuned mass dampers. Aside from outstanding performance in vibration control, these metamaterial turbines incorporate compacted dynamic resonators in their configuration compared to traditional passive controllers. Hence, the proposed design associates small controllers and brings together the concept of multiphysics metamaterials. The paper elaborates on the design and modelling of the turbine metamaterial and the resonators using the dynamic stiffness method. This research underscores the potential of metamaterials to advance wind turbine technology through enhanced vibration control, representing a significant advancement in the design and reliability of wind energy systems.

1. Introduction

The increasing global demand for renewable energy sources, wind energy has emerged as the installation of a sustainable energy harvesting source, such as solar and wind. In particular, wind turbines (WT) have gained attention due to their potential to generate significant amounts of electricity. However, these structures face complex challenges, mainly attributed to vibrations caused by wind, wave, and seismic excitations. Such vibrations can result in structural fatigue, decreased efficiency, and even early failure of the turbines. In response to these challenges, vibration control systems have become a focal point of research and development efforts aiming to enhance the structural integrity and extend the operational lifespan of turbines. Control devices are classified into passive, active, and semi-active controllers. These methods function through dampers, system controllers, and hybrid configurations, with passive control being the most commonly employed for mitigating vibrations in WTs (Xie and Aly, 2020; Machado and Dutkiewicz, 2024b) Passive control systems reduce vibrations by absorbing mechanical energy and dissipating it via dampers, requiring no external power as they rely on the structure's motion to reduce dynamic forces. Those passive devices are split into material-based and inertia-based systems. Material-based controls, such as friction, viscoelastic dampers, and shape memory alloys, are prevalent in wind energy applications. Among the inertia-based systems, the tuned mass dampers (TMD) are favoured for their cost-effectiveness and ease of frequency tuning, tuned liquid dampers (TLD), which use liquid for energy dissipation, provide advantages such as multi-directional vibration control and low maintenance.

The tower and nacelle, the heaviest wind turbine components, are highly prone to wave-wind-induced loads. Researchers have developed vibration control systems targeting all turbine components. For large WTs, optimal TMDs have been employed (Chen et al., 2021a; He et al., 2017; Chen et al., 2021b), TMD and RID-TMD optimisation based on wind distribution (Liu et al., 2021a,b), TMDs and roll cylinder TMDs (Ball-TMD) for floating offshore turbines (Li et al., 2017; Yang et al., 2019; Liao and Wu, 2021), and considering uncertainties due external force (Verma et al., 2022). To address bi-directional

* Corresponding author at: Department of Mechanical Engineering, University of Brasilia, 70910-900, Brasília, Brazil.
E-mail address: marcelam@unb.br (M.R. Machado).

https://doi.org/10.1016/j.egyr.2025.01.003
Received 23 October 2024; Received in revised form 20 December 2024; Accepted 2 January 2025
Available online 23 January 2025

vibrations in monopile WTs, a 3D pendulum-TMD was studied for simultaneous fore-aft and side-to-side control (Sun and Jahangiri, 2018; Jahangiri and Sun, 2022) and for global vibration control (Jahangiri et al., 2021; Colherinhas et al., 2022). At the same time, multiple-TMDs and pendulum absorbers were calibrated for various vibration directions (Zuo et al., 2020). Additionally, a double-response damper, combining TMD with a particle damper, was introduced for wind-induced vibrations in turbine towers (Chen et al., 2018), with further studies on TMDs addressing wind-wave-earthquake loads (Yang et al., 2020; Zhang et al., 2020; Villoslada et al., 2022). Inerter-based solutions were explored for floating offshore turbines and monopile configurations to enhance vibration absorption (Hu et al., 2018; Zhang and Hoeg, 2021; Zhang et al., 2023; Alotta et al., 2023). Ghassempour et al. (2019) show that optimal structural vibration reduction in offshore wind turbines (OWT) depends on wind velocity and constraints during operation, unlike conventional TMDs, which may not be effective in varying operational conditions. Thus, tuned liquid dampers have emerged as a promising solution for controlling wind turbine vibrations over traditional TMD (Konar and Ghosh, 2023b). Full-scale TLDs have effectively mitigated lateral tower vibrations of 2MW and 3MW wind turbines, as demonstrated through real-time hybrid testing (Zhang et al., 2016, 2019a). This research modelled the turbine in those studies as a 13-degree-of-freedom aeroelastic model. Variations of TLD, such as the annular tuned liquid dampers (ATLD), can reduce vibrations through liquid sloshing within a circular enclosure as explored in Ghaemmaghami et al. (2013, 2016). The authors discuss using ATLDs for wind turbines, particularly their performance under seismic events, and analyse numerical implementations for optimal vibration reduction in WT structures. ATLDs with damping screens could enhance the controller's performance by increasing energy dissipation. In McNamara et al. (2021), an improvement in OWT amplitude response reduction is demonstrated compared to the TMD undergoing harmonic force excitation. Spherical-TLDs for vibration control in wind turbines were investigated in Chen and Georgakis (2015) and Chen et al. (2016) by theoretically and through 1/20 scaled experimental test WT models, where shown that spherical TLDs in some cases could improve damping capacity and reduce oscillation by up to 35%. This study also considered damper size, liquid properties, and wind turbine vibration frequencies affecting damper efficiency. Further in Buckley et al. (2018a), a spherical-TLD consisting of two-layer hemispherical containers has been tested on a scaled model, showing a significant reduction in the standard deviation of dynamic response under various loads.

Tuned liquid column dampers (TLCD) have emerged as a promising technology for mitigating the dynamic responses of WT against environmental excitation. The application of TLCDs has been found to contribute significantly to the performance of OWT under the simultaneous action of wind, wave, and seismic loads. This breadth of investigation, encompassing TLCDs for jacket-type OWT, full-scale testing for large turbines (Zhang et al., 2016, 2019a), and the consideration of soil–structure interaction for monopile foundations (Zhang et al., 2015; Buckley et al., 2018b), underscores the versatility and adaptability of TLCDs as a solution to the multifaceted challenge of OWT vibration control. The application of TLCDs has been utilised for multi-hazard excitation control, with analysis demonstrating a significant reduction in system vibration when optimal TLCDs have been proposed in ling Chen and Georgakis (2013), Hemmati et al. (2019) and Colwell and Basu (2009). Another variant of the liquid column damper, the circular liquid column damper (CLCD), has also been proposed for controlling edgewise vibrations, effectively suppressing dynamic responses in wind turbines (Zhang and Hoeg, 2018). Further advancements include the development of semi-active vibration control strategies, which employ magneto-rheological-TLCD (Sarkar and Chakraborty, 2019) for adaptive damping in horizontal axis wind turbine towers, and with H-infinity control (Karimi et al., 2010; Fath et al., 2020). This approach offers the flexibility to adjust the damper's behaviour to varying environmental forces in real-time, potentially enhancing the vibration control capabilities under diverse operational scenarios. Passive toroidal-TLCDs are modelling by finite volume and element methods to control the vibration of monopile wind turbines, providing a deeper insight into the fluid–structure interaction and assisting in designing more efficient damping systems (Ding et al., 2022). The use of tuned liquid column gas dampers (TLCGDs) to control wind-wave-induced vibrations in jacket-type offshore wind turbines showed significant decreases in nacelle displacement and acceleration (ling Chen and Georgakis, 2015; Dezvareh et al., 2016). Studies have demonstrated the TLCDs effectiveness in reducing pitch motion in semisubmersible floating turbine substructures (Xue et al., 2022; Tsao et al., 2023; Sardar and Chakraborty, 2022; Zhang and Hoeg, 2020), which is critical for maintaining the stability and operational integrity of these systems. Therefore, studies on TLDs and similar technologies highlight their potential as efficient solutions for managing vibrations in wind turbines. The size and complexity of construction, installation, and maintenance are still critical to incorporating such systems into the turbine design.

Mechanical metamaterials offer negative stiffness and mass density advantages, which can be optimised for specific frequency ranges to enhance vibration isolation (Hussein et al., 2014; Dalela et al., 2022; Sinha and Mukhopadhyay, 2023). These engineered metamaterials for vibration control are commonly designed as periodic structures, incorporating resonators, masses, geometry, and other distributed features throughout the structure. This arrangement provides superior vibration suppression within bandgap regions, surpassing the capabilities of traditional dynamic absorbers (Brennan, 2006), and effectively manipulates elastic wave propagation for broad vibration isolation (Machado and Dos Santos, 2021; Burlon and Failla, 2022). Based on the mechanical dynamic vibration absorber concept, local resonators have been extensively explored for their effectiveness in various structures. The combination of different materials and physics in resonator design enhances the functional properties of these metamaterials. As a result, multiphysics metamaterials enable the regulation of complex physical processes by integrating multiple physical fields (Lei et al., 2023). Such multifunctional metamaterials allow simultaneous control of electromagnetic and acoustic fields (Zhang et al., 2019b), conductive and convective processes (Xu et al., 2021), as well as thermal and electric fields (Yang et al., 2015; Stedman and Woods, 2017). To improve the efficiency of vibration absorbers, scholars have proposed combining soft and hard materials (Liu et al., 2000; Xu et al., 2019), using soft rubber within epoxy (Wang et al., 2004), embedding soft or hard materials into the substrate (Assouar and Oudich, 2012), and employed electromechanical controllers (B.Moura et al., 2022; Machado et al., 2022; deMoura et al., 2024). In Zhang et al. (2018) and Wu and Li (2021), the authors proposed using a tuned slosh damper resonator. These tunable fluid-solid metamaterials can also control elastic waves across a broad frequency range, essential for applications such as vibration isolation, dynamic tuning of material properties, bandgap frequency adjustment, wave guiding, and energy harvesting.

Complex and large-scale metamaterial structures have benefited from the use of the metamaterial concept in improving vibration reduction capabilities for various engineering applications, including vibration control of stayed bridges employing I-Girder metastructure (Zhong et al., 2018), transverse taut string with mechanical absorber metamaterial (Singleton et al., 2019), prestressed elastic beams (Zhou et al., 2021), overhead transmission cable (Machado and Dutkiewicz, 2024a), water-tank meta barrier (Francesco et al., 2024), and Machado et al. (2024) discussed structural control methods and recent advancements in mitigating vibration issues in wind turbines, highlighting mechanical metamaterials based on TMD resonators for vibration control. By incorporating those functional mechanical metamaterials to control the vibration of large structures, an enhancement in the control and advancements in technology was presented over conventional techniques. Improving the damping factor is still challenging to incorporate in those

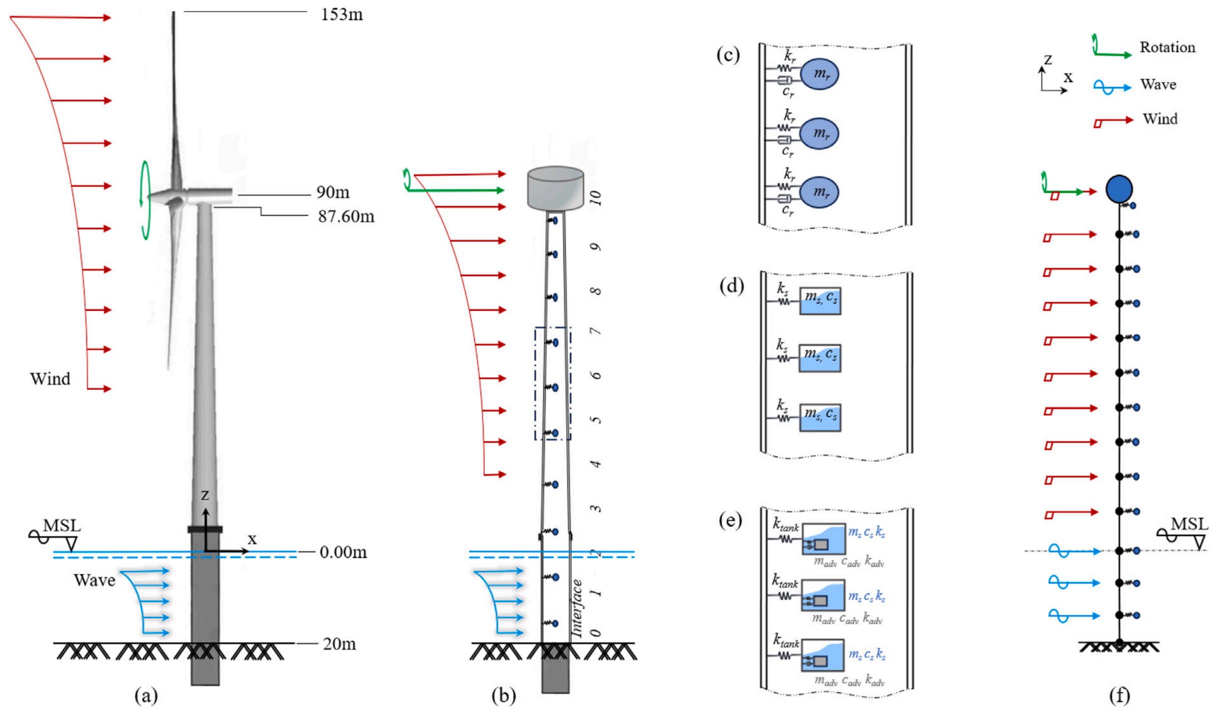

Fig. 1. NREL 5 MW OWT: (a) Schematic representation, including wind, blade rotation and wave forces; (b) Simplified metamaterial WT model considering rotor-nacelle (RNA) as a lumped mass placed at the tower top; (c) Representation of the TMD resonator controller; (d) TSD resonator; (e) Multiphysics resonator; (h) DSM model metamaterial WT.

metastructures without increasing the complexity of the controller's device. Despite numerous applications and models dedicated to passive vibration control of large systems, particularly wind turbines, there is a notable gap in the research literature concerning using metamaterials to mitigate turbine vibration and achieve broadband control spanning single to multiple frequencies. This research direction remains an open challenge that requires thorough investigation.

While passive vibration control methods for wind turbines have been extensively studied, using mechanical metamaterials to address offshore wind turbine vibrations is a largely unexplored area. This paper proposes a novel solution based on mechanical metamaterial composed of multiphysics resonators to enhance vibration control in offshore wind turbines. The unique aspect of this approach is its ability to increase the damping factor without significantly complicating the control system. This research contributes to the design of metamaterial wind turbines, particularly the configuration of TSDs and multiphysics resonators. This novel approach significantly enhances damping and reduces vibration amplitudes in wind turbines' dynamic displacements subjected to hazard forces, demonstrating the control system's effectiveness. Additionally, the spectral modelling of the slosh and multiphysics resonator is detailed and formulated in this study. Various liquids were tested in the slosh configuration to optimise control performance. The effectiveness of the multiphysics resonators in reducing vibration amplitudes is demonstrated by combining fluid energy dissipation with the solid oscillating structures. Furthermore, the practical application of this research is significant in the wind energy field, where the scalability and adaptability of this metamaterial turbine design are associated with the reduced size weight of the resonators and the increasing displacement amplitude attenuation, decreasing costs of maintenance and system downtime. The proposed control's efficiency was evaluated under wind, wave, and blade rotation loads, simulating the operational conditions of offshore wind turbines. Results indicate that the multiphysics metamaterial-based offshore wind turbine achieved up to a 60% reduction in vibration amplitude under multi-hazard excitation compared to only 7.8% with the traditional TMD method, emphasising its potential for practical applications across diverse environmental conditions. Overall, the paper is organised as follows: Section 2 the wind turbine metamaterial modelled using the dynamic stiffness matrix and in Section 3 dynamic formulation of the TMD, TSD and multiphysics resonators. Sections 4 and 5 showcase the numerical results and evaluation, followed by the conclusion in Section 6 and supplementary material. Multiple hazard excitation, such as wind-wave loading, follows the specification by IEC 61400-1 (IEC and IEC 61400-1, 2005).

2. Metamaterial wind turbine for locally resonant frequency attenuation

Mechanical and acoustic metamaterials are specially designed materials or structures that use embedded resonators or similar devices to control vibrations. These resonators create a bandgap (for infinite structures) or attenuation bands (for finite structures) in a specific frequency range where elastic waves cannot propagate. This effect isolates unwanted vibrations, making metamaterials highly effective for reducing noise and improving stability in mechanical systems. Different from traditional methods, such as the classical TMDs or TLDs, they do not rely on precise placement, offering a lightweight and versatile solution for vibration control in various applications, aside from effectively reducing the controllers' size.

The dynamic stiffness method (DSM) (Doyle, 1997; Lee, 2009) presents an alternative approach to dynamic simulation and analysis. The analytical solution of the wave equation used in the element shape function formulation enables high precision while requiring only a few elements, often a single one, to model uniform structural sections. This feature of the DSM ensures computational efficiency, outperforming traditional finite element methods (FEM) by eliminating the need for fine meshing. Unlike FEM, DSM models continuous structures directly, making it particularly effective for long systems such as wind turbine towers and blades, which results in substantial computational efficiency as shown in Colherinhas et al. (2022). Temporal responses, a good representation for evaluating vibration control, can be readily obtained from frequency-domain solutions using inverse Fourier transformation. The adoption of DSM for modelling wind turbines and their controllers is justified by its ability to reduce computational effort, maintain accuracy in dynamic solutions, and naturally incorporate the

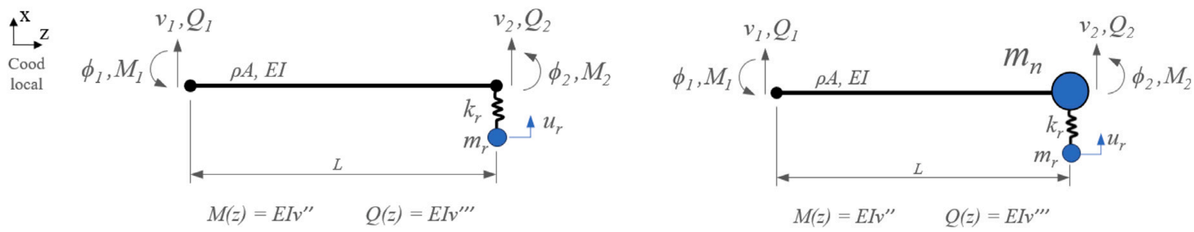

(a) (b)

Fig. 2. Nodal displacements and forces for the beam elements employed in the metamaterial wind turbine modelling. (a) Beam with attached resonator and (b) beam with attached resonator and lamped mass. The elements are formulated in the local coordinates referring to the plane x-z. The global coordinates assumed the turbines coordinate plane Z-X.

spectral characteristics of wind, waves, and blade rotation dynamic loads. Furthermore, DSM offers a wave-like interpretation of structural dynamics, which opens up possibilities for innovative wave-based control strategies. A two-dimensional spectral model of the monopile NREL 5 MW turbine (Jonkman et al., 2009) is modelled using DSM, similar to the proposed and validated in Machado et al. (2024). The tower and monopile are modelled by the beam element and, for model simplification, the rotor-nacelle (RNA) as a lumped mass, shown in Fig. 1(a). The validation of the spectral model is given in supplementary material, Appendix.

The metamaterial wind turbine employing dynamic absorbers for vibration control, illustrated in Fig. 1(b–f), is then incorporated into the DMS element formulation. In general, the global coordinates in the wind turbine for the fore-aft vibration are commonly assumed in the plane Z-X (Fig. 1). The spectral formulation is assumed in the local coordinate x-z as identified in Fig. 2. The equation of motion for the beam with attached tuned mass damper resonator shown in Fig. 2(a) is formulated by applying Hamilton's Principle, which is formulated by the variations of kinetic energy ($\delta\mathtt{T}$), potential energy ($\delta\mathtt{U}$), and the virtual work ($\delta\mathtt{W}$) performed by the concentrated harmonic load as

$$\int_{t1}^{t2} [\delta(\mathtt{T}-\mathtt{U}) + \delta\mathtt{W}]\delta t = 0 \tag{1}$$

$$\delta\mathtt{U} = \int_0^L EI\frac{\partial^2 v}{\partial z^2}\delta\frac{\partial^2 v}{\partial z^2} + \sum_{r=1}^{\bar{n}} k_r(v-u_r)\delta(z-z_r)dz + \sum_{r=1}^{\bar{n}} k_r(u_r - v_{zr})\delta u_r,$$

$$\delta\mathtt{T} = \int_0^L \rho A\frac{\partial v}{\partial t}\delta\frac{\partial v}{\partial t}dz + \sum_{r=1}^{\bar{n}} m_r\frac{\mathrm{d}u_r}{\mathrm{d}t}\delta\frac{\mathrm{d}u_r}{\mathrm{d}t}, \qquad \delta\mathtt{W} = \int_0^L F\delta(z-z_f)\delta v dz$$

where the δ is used to represent the variation of the energies, and the Dirac delta $\delta(z)$ represents the position of each resonator. Substituting the variations of the energies into Eq. (1), yields

$$\int_{t_1}^{t_2}\left[\int_0^L EI\frac{\partial^2 v}{\partial z^2}\delta\frac{\partial^2 v}{\partial z^2} + \sum_{r=1}^{\bar{n}} k_r(v-u_r)\delta(z-z_r)dz + \sum_{r=1}^{\bar{n}} k_r(u_r-v_{zr})\delta u_r \right.$$
$$\left. - \int_0^L \rho A\frac{\partial v}{\partial t}\delta\frac{\partial v}{\partial t}dz + \sum_{r=1}^{\bar{n}} m_r\frac{\mathrm{d}u_r}{\mathrm{d}t}\delta\frac{\mathrm{d}u_r}{\mathrm{d}t} + \int_0^L F\delta(z-z_f)\delta v dz\right] dt = 0 \tag{2}$$

In the variational approach, the weak form of the metamaterial beam attached to the resonator equation of motion is evaluated under the weighted-integral statement in an arbitrary variation of the displacement v. Assume there are $\bar{n}$-resonators attached to the beam at locations v_{z_r}, with masses m_r, stiffness k_r, natural frequencies $\omega_r^2 = k_r/m_r$, and relative displacements u_r, Eq. (2) can be rewritten in frequency domain as

$$\int_{t_1}^{t_2}\left[\int_0^L EIv''\delta v'' - \omega^2\int_0^L \rho A v\delta v - \sum_{r=1}^{\bar{n}} m_r\omega_r^2 u_r\delta(z-z_r)dz \right.$$
$$\left. - \int_0^L F\delta(z-z_f)\delta v dz\right] dt = 0 \tag{3a}$$

$$\int_{t_1}^{t_2}\left[\sum_{r=1}^{\bar{n}} m_r\frac{\mathrm{d}^2u_r}{\mathrm{d}t^2} + k_r(u_r - v_{z_r})\right] dt = 0 \tag{3b}$$

where $'$ denotes space derivation. By considering the nodal displacements $\boldsymbol{d} = [v_1, \phi_1, v_2, \phi_2]^T$, and forces $\boldsymbol{f_c} = [Q_1, M_1, Q_2, M_2]^T$, a assumed solution $v(z) = \boldsymbol{g}(z,\omega)\boldsymbol{d}$, and substitution in Eq. (3a) it gives,

$$\delta\boldsymbol{d}^T\left[\int_0^L\left(EI\boldsymbol{g}''^T(z,\omega)\boldsymbol{g}''(z,\omega) - \omega^2\int_0^L \rho A\boldsymbol{g}^T(z,\omega)\boldsymbol{g}(z,\omega)\right.\right.$$
$$\left.\left. - \sum_{r=1}^{\bar{n}} m_r\omega_r^2 u_r\delta(z-z_r)dz\right)\boldsymbol{d} - (\boldsymbol{f}_c + \boldsymbol{f}_d)\right] = 0 \tag{4}$$

where $\delta\boldsymbol{d}$ is arbitrary by definition (Lee, 2009), and the nodal forces are defined by

$$\boldsymbol{f}_d(\omega) = \int_0^L F(z,\omega)\boldsymbol{g}''^T(z,\omega) \tag{5}$$

hence, the dynamic stiffness matrix of the metamaterial beam with the attached resonator is expressed by

$$\boldsymbol{D}(\omega) = EI\int_0^L \boldsymbol{g}''^T(z,\omega)\boldsymbol{g}''(z,\omega)dz$$
$$-\omega^2\rho A\int_0^L \boldsymbol{g}^T(z,\omega)\boldsymbol{g}(z,\omega) - \sum_{r=1}^{\bar{n}} m_r\omega_r^2 u_r\delta(z-z_r)dz \tag{6}$$

and the solution of Eq. (3b) gives the general form of the equation of motion for each resonator in physical coordinates as

$$\frac{\mathrm{d}^2u_r}{\mathrm{d}t^2} + \omega_r^2 u_r + \frac{\mathrm{d}^2 v_{r_z}}{\mathrm{d}t^2} = 0, \qquad r = 1,2,\ldots,\bar{n} \tag{7}$$

The dynamic stiffness matrix elements are formulated in the frequency domain, where the spectral solution for the primary displacement field variables can be obtained by using the Discrete Fourier Transform (DFT) for the temporal field expressed as

$$\boldsymbol{v}(z,t) = \sum_{n=1}^{N}\boldsymbol{v}(z,\omega_n)e^{-\omega_n t} = \sum_{n=1}^{N}\left(\sum_{j=1}^{4}\hat{\boldsymbol{v}}_j e^{ik_j z}\right)e^{i\omega_n t} \tag{8}$$

where $i = \sqrt{-1}$, ω_n is the circular frequency at nth sampling point, k_j the wavenumber, $\boldsymbol{v}_j$ the displacements, and N is the Nyquist point in DFT. Thus, the element spectral shape function $\boldsymbol{g}(z,\omega)$ is formulated given the frequency domain, and the spectral displacements yields

$$\hat{v}(z) = \sum_{j=1}^{4} a_j e^{-ik_j z} = \mathbf{s}(z,\omega)\mathbf{a}, \qquad \mathbf{s}(z,\omega) = [e^{-ik_1 z}, e^{-ik_2 z}, e^{-ik_3 z}, e^{-ik_4 z}],$$
$$\mathbf{a} = [a_1, a_2, a_3, a_4]^T \tag{9}$$

with the frequency-dependent displacement within an element is interpolated from the nodal displacement vector $\boldsymbol{d}$ the shape function is described by

$$\mathbf{g}(z,\omega) = \mathbf{s}(z,\omega)\boldsymbol{\Gamma}(\omega) \tag{10}$$

$$\boldsymbol{\Gamma}(\omega) = \begin{bmatrix} 1 & 1 & e^{-ikL} & e^{-kL} \\ -ik & -k & kie^{-ikL} & ke^{-kL} \\ e^{-ikL} & e^{-kL} & 1 & 1 \\ -kie^{-ikL} & -ke^{-kL} & ik & k \end{bmatrix}^{-1}$$

where $k = \omega(\rho A/EI)^{1/4}$ is the wavenumber. The matrix $\boldsymbol{\Gamma}(\omega)$ is obtained by considering a finite element with length L, the spectral nodal displacements in terms of a_j, which satisfy the boundary conditions of the system, where the spectral nodal displacements ($\hat{v}$) and slopes ($\hat{\phi} = \hat{v}'$) are obtained at the nodes so that at node 1 (left end, $z = 0$) and node 2 (right end, $z = L$) (Doyle, 1997; Lee, 2009).

The OWT model by DSM illustrated in Fig. 1(f) assumes wind, rotation of the blades (1P), and wave spectral excitation. The OWT NREL 5MW monopile (Jonkman et al., 2009) features a tower with a tapered geometry, assuming a top diameter of 3.87 m and a base diameter of 6 m. In this study, we modelled the monopile tower's tapered shape by gradually reducing the cross-sectional area of each beam element from the bottom (element one) to the top. The base elements (three in total) have a uniform cross-section with a diameter of 6 m, while the diameter and thickness proportionally decrease as the cross-section tapers towards the top. The last element (number 13) corresponds to the top diameter. The model comprises a mesh with 13 elements formulated in Eq. (6). The simplified OWT model assumes the RNA is a lumped mass on the tower top. Therefore, the last element considers the RNA-concentrated mass as shown in Fig. 2(b) in its formulation and the kinetic energy, which is described as

$$\delta \mathrm{T} = \int_0^L \rho A \frac{\partial v}{\partial t} \delta \frac{\partial v}{\partial t} + m_n \delta(z-L) \frac{\partial^2 v}{\partial t^2} dz + \sum_{r=1}^{\bar{n}} m_r \frac{\mathrm{d}u_r}{\mathrm{d}t} \delta \frac{\mathrm{d}u_r}{\mathrm{d}t} \tag{11}$$

where the lumped mass assumes $\tilde{m}_n = m_n / EI\beta^3$ at position $z = L$. The material properties are defined by E, I, ρ, and A is Young's modulus, inertia moment, mass density, and cross-section area, respectively. The hysteretic damping is introduced into the element formulation by adding the complex Young's modulus so that $E = E^*(1 + i\eta)$, where $\eta = 0.01$ is the damping factor. While structural damping influences the entire dynamic response, the local control, as the resonator, is designed to induce a pronounced dynamic response, specifically at the control targets' desired mode shapes and resonant frequencies. By substituting Eq. (11) in (1) and assuming similar consideration to the beam-resonator element, the dynamic stiffness matrix beam-resonator-mass element is given by

$$\begin{aligned} \boldsymbol{D}(\omega) = EI \int_0^L & \boldsymbol{g}''^T(z,\omega)\boldsymbol{g}''(z,\omega) dz \\ & - \omega^2 \rho A \int_0^L \boldsymbol{g}^T(z,\omega)\boldsymbol{g}(z,\omega) + \tilde{m}_n \delta(z-L) - \sum_{r=1}^{\bar{n}} m_r \omega_r^2 u_r \delta(z - z_r) dz \end{aligned} \tag{12}$$

where $\tilde{m}_n = m_n / EI\beta^3$, $\delta(z-L)$ is Dirac's delta at $z = L$. The unit cell of the system for dynamic modelling considers each element of the mesh. The wind turbine modelling considers the element assembly in the global matrix ($\mathbf{D}_G(\omega)$) as the conventional finite element method. In Machado et al. (2024), the authors used the tuned mass damper-like resonator in the wind metamaterial configuration. Therefore, in this paper, we adopted the slosh and hybrid multiphysics type of resonator formulated in Section 3. The general representation of the metamaterial global stiffness dynamic matrix assembly that considered different types of dynamic absorbers, which in this application assumed the beam element attached to the chosen resonator at its right end, is given as

$$\begin{aligned} &\mathbf{D}_G(\omega) = \sum_{e=1}^{tot} \mathbf{D}(\omega), \qquad \mathbf{D}(\omega) = \begin{bmatrix} \mathbf{D}_{\mathrm{ll}} & \mathbf{D}_{\mathrm{lr}} \\ \mathbf{D}_{\mathrm{rl}} & \mathbf{D}_{\mathrm{rr}} + \mathbf{D}_0 \end{bmatrix}, \\ &\mathbf{D}_{\mathrm{ll}} = \begin{bmatrix} D^{11}(\omega) & D^{12}(\omega) \\ D^{21}(\omega) & D^{22}(\omega) \end{bmatrix}, \quad \mathbf{D}_{\mathrm{lr}} = \mathbf{D}_{\mathrm{rl}}^T = \begin{bmatrix} D^{13}(\omega) & D^{14}(\omega) \\ D^{23}(\omega) & D^{24}(\omega) \end{bmatrix}, \\ &\mathbf{D}_{\mathrm{rr}} = \begin{bmatrix} D^{33}(\omega) & D^{34}(\omega) \\ D^{43}(\omega) & D^{44}(\omega) \end{bmatrix}, \quad \mathbf{D}_0 = \begin{bmatrix} 0 & 0 \\ 0 & D_0(\omega) \end{bmatrix} \end{aligned} \tag{13}$$

the subscripts l and r denote the left and right sides of the unit cell assuming the dynamic condensed description, tot is the number of elements assumed in the mesh, the $D(\omega)$ defines the spectral element matrix component obtained by solving the Eqs. (6) and (12), and $D_0(\omega)$ the resonator, which is defined in Eq. 3.1 and detailed defined in Section 3.

2.1. Multiple loads excitation

The offshore wind turbine is exposed to various hazardous loads, including rotating blades, waves, and along-wind forces, as illustrated in Fig. 1(c). The combination of those spectra composes the multi-load excitation. In this study, a wind velocity of $V_{\mathrm{hub}} = 12$ m/s is assumed, serving as input for estimating ten Kaimal power spectrum density (PSD) calculated at equidistant points along the turbine, ranging from the Still Water Level (SWL) up to the top. A slight degree of randomness is introduced into the Kaimal PSD following the IEC specifications (IEC, 2005) and DNV-OS-J101(Det Norske Veritas, 2014), adding stochasticity to the spectrum. The JONSWAP PSD (IEC, 2005) considers a wave height of $H_s = 6$ m and a wave period of $T_p = 10$ s in the fore-aft direction of the baseline OWT. The rotational effects of the RNA are assumed in the model by using the blade root bending moment spectrum, which assumes a rotor rotation frequency of 12.1 rpm (Burton et al., 2001). These external vibration sources are stochastically simulated based on the theories described in detail see Machado et al. (2024) and Colherinhas et al. (2022), and in the supplementary material in Appendix.

The relation used in the analysis of the dynamic response of any system to random or spectral excitation is that the auto-spectral density (PSD) of the response of a system, $PSD(\omega)$, to an excitation input $PSD_{fo}(\omega) = PSD_{wind}(\omega) + PSD_{wave}(\omega) + PSD_{rotation}(\omega)$ is given by

$$PSD(\omega) = |\mathbf{H}(\omega)|^2 \quad PSD_{fo}(\omega) \tag{14}$$

where the function $\mathbf{H}(\omega) = \mathbf{D}_G^{-1}(\omega)$ is the transfer function of the dynamic response.

3. Spectral design of the metamaterial's resonators

The use of dynamic vibration absorbers as a passive method for reducing vibrations in wind turbines is widespread due to their simplicity and effectiveness (Machado and Dutkiewicz, 2024b). Depending on the construction, those dynamic systems are characterised by the TMD and TLD categories. They generally operate up to two resonant frequencies simultaneously, and their efficacy depends on their placement and overall features within the structure. This passive control relies on the system's inherent damping and stiffness properties and is an energy-dissipating device without additional power sources. The control is activated by vibrations from the primary structure to which it is attached, making it cost-effective and easy to maintain, among other benefits. Hence, those passive energy dissipation devices are widely used for vibration control due to their simplicity and reliability, as they do not require electronics or actuators. However, they have limitations such as a narrow operating frequency range, specific material properties for damping, and lack of real-time frequency control adjustability.

TLD has an advantage over TMD regarding activation requirements, external damping elements, frequency tuning, and multi-directional vibration control with a single device (Konar and Ghosh, 2023b). Additional damping parameters like viscous, viscoelastic, friction, and fluid damping types can significantly enhance the efficacy of passive controllers. The damping coefficient is crucial in mitigating vibrations and improving system stability across various engineering applications. Passive components' simplicity and reliability can be leveraged to manage vibrations and improve the overall performance of different systems. In this study, we investigate three types of resonators periodically attached to the metamaterial wind turbine, and the TMD used as a reference once previews formulated and validated in Machado et al. (2024), tune slosh damper (TSD), and the multiphysics resonators consisting of the TMD combined with TSD, respectively, as shown in Fig. 3(a–c).

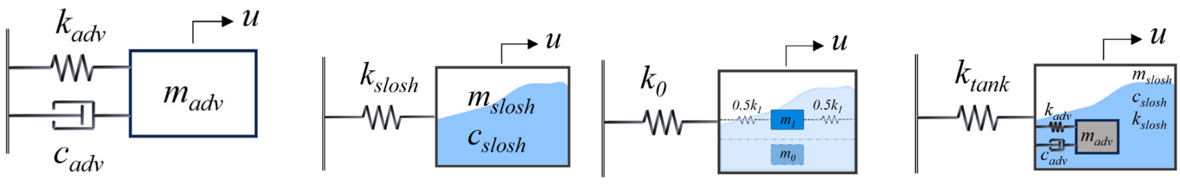

Fig. 3. Resonators representation: (a) TMD, (b) TSD formulated with hydrodynamic (LHS) and equivalent mechanical model theory (RHS) and (c) hybrid resonator.

3.1. Tuned mass damper resonator

The resonant frequencies of the OWT are clearly defined and are spaced at distinct intervals. The control mechanisms and their specific characteristics are described separately, with the resonator configurations illustrated in Fig. 3(a). Within the OWT metamaterial, a total of N resonators are positioned in a specified subdomain, where $\Delta L_j = \int_{L_j} dL$ represents the length of the subdomain L_j. The spring coefficient for each resonator (k_r) is considered uniform. In contrast, the mass of each resonator is given by $m_r = \epsilon m \Delta L$ (Sugino et al., 2016), where the mass ratio is defined as $\epsilon = \sum^{N} p = 1mr / \int_L m(x) dL$, with $m(x)$ representing the mass density at a specific point in the domain. The equation of motion governing the resonators is

$$\ddot{u}_r(t) + \omega_r^2 u_r(t) + \ddot{v}(z,p,t) = 0, \qquad \omega_r = \sqrt{\frac{k_r}{m_r}}, \qquad r = 1,2,\ldots,N$$

where ω_r is the resonator tuned frequency, $v(z,r,t)$ is the displacement of a point with position vector in z of the primary structure, and $u_r(t)$ the displacement of the rth resonator. The relative displacement expressed by $u_r = (\mathrm{u}_r - v_{z_p})$, represents the displacement of each resonator rth concerning the relative displacement of the principal structure (v_{z_r}). Hysteretic damping is considered for the resonator springs, where $k_r = \bar{k}_r(1 + i\zeta)$, as this model is typically linked to dry friction occurring within the material. Generalising governing equation of the resonator is expressed as

$$\begin{bmatrix} 0 & 0 \\ 0 & m_r \end{bmatrix} \begin{bmatrix} \ddot{v}_z \\ \ddot{u}_r \end{bmatrix} + \begin{bmatrix} k_r & -k_r \\ -k_r & k_r \end{bmatrix} \begin{bmatrix} v_z \\ u_r \end{bmatrix} = \begin{bmatrix} f_0 \\ 0 \end{bmatrix} \tag{15}$$

where v_z is the displacement of the attachment point on the primary structure, and f_0 is the reaction force from the primary structure. Eq. (15) is dynamically condensed to express the dynamic stiffness of the resonator as (Xiao et al., 2013)

$$D_0(\omega) = \frac{k_r - k_r^2}{(k_r - \omega^2 m_r)} \tag{16}$$

3.2. Tuned sloshing damper resonator in cylindrical tank

Tuned slosh dampers, a type of TLD (Konar and Ghosh, 2023b), are a form of passive inertia-based dissipation device within the damper category. TSD employs liquid as either the primary or partial mass for damping, facilitating energy dissipation without needing specific external excitation thresholds for activation, eliminating the requirement for an external damping component, and allowing the management of vibrations in multiple directions using a single device. Sideway sloshing refers to the movement of the liquid surface within an upright container when subjected to lateral stimulation, generating asymmetric mode shapes. TSD containers come in various shapes, with the TSD's auxiliary system mass consisting entirely or partially of liquid, actively participating in energy dissipation. To function effectively as an inertia-based damper, TSD must align its frequency with the specific structural mode requiring control, with the control frequency related to the motion frequency of the liquid, and in the same configuration as with the submerged part.

Approaching sloshing problems typically involves two distinct methods, one employing linearised hydrodynamic theory (Abramson et al., 1961; Roberts et al., 1966) focused on the velocity potential function to derive the natural frequency of the sloshing liquid and the other utilising equivalent mechanical model to represent the sloshing problem (Ocak et al., 2022; Sharma et al., 2019). This paper investigates both theories, briefly outlined in the present section.

3.2.1. Hydrodynamic theory

The theoretical hydrodynamic formulation of the sloshing can prove challenging due to the complex nature of the free surface formed by the sloshing liquid, as shown in Fig. 4(a). To simplify, several assumptions are made (Ibrahim, 2005; Sharma et al., 2019): (i) the tank containing the liquid is considered rigid to avoid complications arising from container flexibility; (ii) the heights of free surface waves are assumed small to linearise the problem; (iii) the liquid is presumed incompressible, irrotational, homogeneous, and inviscid; and (iv) the total volume of liquid inside the tank remains constant. For the conventional TSD in the circular tank, a similar equation of motion of Eq. 3.1 is assumed with a lateral force acting on the walls of the tank by sloshing liquid due to a pure translation excitation, represented by $X = x_0 \sin(\omega t)$. In this case, the equivalent mass (m_s), stiffness (k_s) and damping (c_s)parameters for the first mode of sloshing given by Abramson (1966)

$$m_s = M_{tl} \frac{\pi \rho_l R^3}{2.2} \tanh\left(\frac{1.84h}{R}\right), \qquad k_s = M_{tl} \frac{1.85g}{R} \tanh\left(\frac{1.84h}{R}\right),$$
$$c_s = \zeta_s 2\sqrt{m_s k_s} \tag{17}$$

where $M_{tl} = m_0 + m_1$, denoting the total mass of liquid inside the tank (passive mass m_0 plus the active mass m_1), and the damping rate of the sloshing liquid is (Abramson, 1966; Bauer, 1962; Sharma et al., 2019)

$$\zeta_s = 4.98 \nu^{1/2} R^{-3/4} g^{-1/4} \left[1 + \frac{0.18}{\sinh\left(\frac{1.84h}{R}\right)} \frac{1 - \frac{h}{R}}{\cosh\left(\frac{1.84h}{R}\right)} \right] \tag{18}$$

where ν is the kinematic viscosity of the fluid, h and R denote the height and radius of the cylindrical tank, respectively, g the gravity, and ρ_l the density of the liquid. The equivalent first natural frequency of sloshing is provided by

$$\omega_s^2 = \frac{1.84g}{R} \tanh\left(\frac{1.84h}{R}\right) \tag{19}$$

The equation of motion for the slosh hydrodynamic theory follows Eq. (15), where the dynamic representation of the slosh resonator yields

$$D_0(\omega) = \frac{k_s - k_s^2}{(k_s - \omega^2 m_s)} \tag{20}$$

The design of TSD aims for the best damper performance related to the expected loading and desired frequency. The optimised parameters for achieving the control frequency are primarily associated with the slosh equivalent mass and stiffness (Eq. (17)). These parameters depend on the mass ratio, which is determined by the tank's geometry, liquid level, and properties. This study conducted an optimisation procedure by fixing the mass ratio and liquid properties and exploring ranges for the tank's geometric ratio and liquid level to identify the optimal values that yield the desired control frequency. The optimisation process, similar to other algorithms, defines the objective function of the problem, the design constraints, and the lower and upper limit values. The error function is the absolute difference between the desired frequency (ω_d)

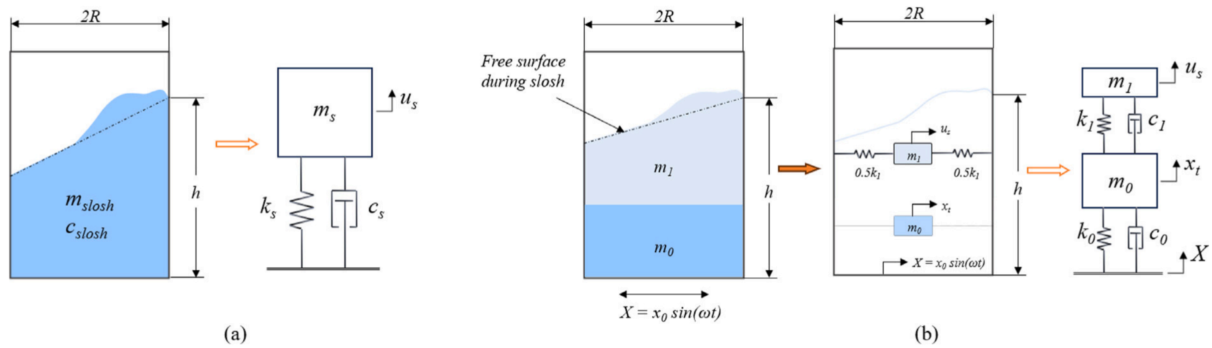

Fig. 4. Schematic representation of the tuned slosh damper: (a) Hydrodynamic approach based on a single-degree-of-freedom dynamic system; (b) Equivalent mechanical model of the sloshing dynamic behaviour based on a two-degree-of-freedom system.

and the frequency derived from the sloshing theory expressed by

$$Error(R) = |\omega_d - \omega_s(R)|, \qquad R_{opt} = \arg\min_R Error(R), \qquad Rmin \leq R \leq Rmax \tag{21}$$

where the value of R_{opt} is calculated by minimising the error function in an interval range as $Rmin = 0.1$m and $Rmax = 1.5$m. The liquid level is then defined by $h = V/\pi R_{opt}^2$, for $V = M/\rho$.

3.2.2. Equivalent mechanical model

The equivalent mechanical mode has been idealised as a two-degree of freedom (Sharma et al., 2019) and three-degree of freedom (Ocak et al., 2022). This paper assumes the two degrees of freedom spring-mass-damper system (Fig. 4 b) for representing the tank sloshing damper and employs the approach presented in Sharma et al. (2019). This model incorporates stiffness (k_0, k_1) and damping (c_0, c_1) directly related to the desired control frequency to describe interactions and uses coupled equations of motion derived from Newton's second law to predict the system's response. By accounting for the beat phenomenon and using the dynamic parameters, the model simplifies the parameter estimation and eliminates the optimisation procedure. It reduces reliance on computational simulations and aids in faster design processes. Hence, the parameters of the proposed model are straightforwardly calculated using the analytical expressions of Eq. (24). The equations of motion for the equivalent mechanical model are derived using Newton's second law of motion as,

$$\begin{aligned} &m_0\ddot{u}_s + k_0(u_s - X) + c_0(\dot{u}_s - \dot{X}) - k_1(x_1 - u_s) - c_1(\dot{x}_1 - \dot{u}_s) = 0 \\ &m_1\ddot{x}_1 + k_1(x_1 - u_s) + c_1(\dot{x}_1 - \dot{u}_s) = 0 \end{aligned} \tag{22}$$

where the steady state, Eq. (22), in matrix form yields

$$\begin{bmatrix} m_0 & 0 \\ 0 & m_1 \end{bmatrix} \begin{bmatrix} \ddot{u}_s \\ \ddot{x}_1 \end{bmatrix} + \begin{bmatrix} c_0 + c_1 & -c_1 \\ -c_1 & c_1 \end{bmatrix} \begin{bmatrix} \dot{u}_s \\ \dot{x}_1 \end{bmatrix} + \begin{bmatrix} k_0 + k_1 & -k_1 \\ -k_1 & k_1 \end{bmatrix} \begin{bmatrix} u_s \\ x_1 \end{bmatrix} = \begin{bmatrix} k_0 X + c_0 \dot{X} \\ 0 \end{bmatrix} \tag{23}$$

In this case, the liquid mass is divided into m_0 and m_1, as shown in Fig. 4(b), representing the active and passive liquids. The liquid that expresses the moving mass in the system is called agitation fluid, while the inert mass is specified as the passive liquid that does not participate in the sloshing (Abramson, 1966). The dynamic representation of the slosh lies in a two-degree freedom system composed of a spring-mass-damper system (Fig. 4b-RHS). The mass of the tank and the mass of the passive liquid are combined and expressed by m_0 as

$$m_0 = M_{tank} + M_{tl} - m_1, \qquad k_0 = m_0(2\pi f_0)^2, \qquad c_0 = 2\zeta\sqrt{m_0 k_0} \tag{24}$$

where M_{tank} is the mass of tank and $m_1 = m_s$ is the sloshing mass. The sloshing mass, stiffness $k_1 = k_s$ and slosh damping $c_1 = c_s$ values are calculated as described in Eq. (17). Additionally, the parameters k_0 and c_0, are incorporated to represent the TSD stiffness and damping of m_0, the damping ratio ζ is assumed to be the hysteretic damping factor. The response of the sloshing mass of liquid is represented by u_s, and the response of m_0 is given by x_1 (Fig. 4b). The condensed form of the equation of motion for multiple-DOFs yields

$$D_0(\omega) = \sum_{r=1}^{\bar{n}} \frac{k_r - k_r^2}{(k_r - \omega^2 m_r)} \qquad r = 0, 1, \ldots \bar{n} \tag{25}$$

where the local resonators with multiple degrees of freedom ($\bar{n}$–DOF) can be attached to the primary structure (El-Borgi et al., 2020; Machado and Dutkiewicz, 2024a).

3.3. Multiphisics tuned damper resonator

The hybrid multiphysics-tuned damper resonator combines elements from both TMD and TSD into a single system. This fluid–structure system involves multiphysics interaction in which the TMD experiences loads from fluid flow, leading to structural displacements and oscillations that, in turn, affect the fluid's motion. In this setup, a tuned oscillator is attached to the tank at deep or intermediate depths. This integration of control mechanisms, initially proposed in Xu et al. (2018), Fu et al. (2018), Konar and Ghosh (2023a), ensures that the oscillator remains submerged in the sloshing liquid, allowing energy dissipation during vibrations. When subjected to lateral excitation, the oscillator initiates vibrations, and the surrounding liquid interacts with it through added mass and viscous drag. As a result, the natural frequency of the submerged oscillator, rather than the liquid sloshing frequency, is adjusted to match the dominant frequency of the primary structure. This characteristic is particularly advantageous for stiff structures where aligning the liquid sloshing frequency with the structural frequency may not always be feasible.

The numerical dynamic model, conceptualised in Xu et al. (2018), Fu et al. (2018), comprises a finite element model implemented in the commercial software ANSYS Workbench. The authors assume an implicit two-way coupling approach to simulate the fluid-solid interaction between the oscillator and the interior two-phase fluid in the combined damper. In Konar and Ghosh (2021, 2023a), the authors proposed a cylindrical pendulum and a plate, both submerged and suspended in a rectangular tank. Analytical solutions are formulated in both papers. The proposed hybrid controller follows the concept introduced in Xu et al. (2018), Fu et al. (2018) and Konar and Ghosh (2021, 2023a). Therefore, in our approach, the immersed oscillator is submerged in a circular tank and follows the explicitly analytical formulation presented in this section. Fig. 5 (a-b) illustrates the schematic representation of the hybrid tuned resonator. At the same time, Fig. 5(c) depicts the dynamic model consisting of a three-degree freedom system, where the slosh and TMD resonator operate in parallel and series with the tank-passive mass.

The formulation of the hybrid tuned damper did not account for structural damping, although it is recognised in real-world devices.

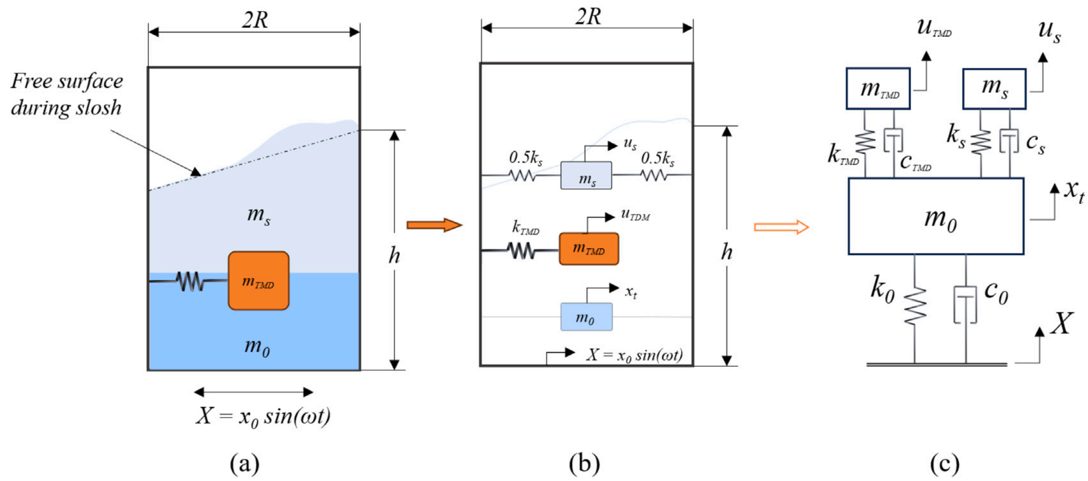

Fig. 5. Schematic representation of the hybrid tuned resonator: (a) ideal slosh resonator, (b) dynamic component of the idealised resonator, and (c) dynamic model consisting of a three-degree freedom system, where the slosh and TMD resonator operate in parallel and series with the tank-passive mass.

Therefore, the focus here is on evaluating the combined damper's effectiveness in damping structures that lack sufficient inherent damping, with particular emphasis on dissipating energy from sloshing liquid. It is also assumed that the illustrated system experiences minimal free horizontal vibration (refer to Fig. 5) and structural deformation. The movements of both the tank and the damper can be described as follows

$$\begin{aligned} &m_0\ddot{x}_1 + k_0(x_1 - X) + c_0(\dot{x}_1 - \dot{X}) + k_s(x_1 - u_s) - c_1(\dot{x}_1 - \dot{u}_s) \\ &+ k_{TMD}(x_1 - u_{TMD}) - c_{TMD}(\dot{x}_1 - \dot{u}_{TMD}) = 0 \\ &m_s\ddot{u}_s + k_s(u_s - x_1) + c_s(\dot{u}_s - \dot{x}_1) = 0 \\ &m_{TMD}\ddot{u}_{TMD} + k_{TMD}(u_{TMD} - x_1) + c_{TMD}(\dot{u}_{TMD} - \dot{x}_1) = F_d \end{aligned} \tag{26}$$

with the steady state, Eq. (26), in matrix form yields

$$\begin{bmatrix} m_0 & 0 & 0 \\ 0 & m_s & 0 \\ 0 & 0 & m_{TMD} \end{bmatrix} \begin{bmatrix} \ddot{x}_1 \\ \ddot{u}_s \\ \ddot{u}_{TMD} \end{bmatrix} + \begin{bmatrix} c_0 + c_s + c_{TMD} & -c_s & -c_{TMD} \\ -c_s & c_s + c_{TMD} & 0 \\ -c_{TMD} & 0 & c_{TMD} \end{bmatrix}$$
$$\begin{bmatrix} \dot{x}_1 \\ \dot{u}_s \\ \dot{u}_{TMD} \end{bmatrix} + \begin{bmatrix} k_0 + k_s + k_{TMD} & -k_s & -k_{TMD} \\ -k_s & k_s + k_{TMD} & 0 \\ -k_{TMD} & 0 & k_{TMD} \end{bmatrix} \begin{bmatrix} x_1 \\ u_s \\ u_{TMD} \end{bmatrix} = \begin{bmatrix} k_0 X + c_0 \dot{X} \\ 0 \\ F_d \end{bmatrix}$$

where m_0, k_0, and c_0 are parameters representing the tank-passive liquid defined in Eq. (24); $m_s = m_1$, $k_s = k_1$, and $c_s = c_1$ are mass, stiffness, and damping of the slosh formulated in Section 3.2; and m_{TMD}, k_{TMD} and c_{TMD} denote mass, damping, and stiffness of the tuned oscillator, expressed in Section 3.1. The variables x_1, u_s, and u_{TMD} are the displacements of each mass. The drag force characterises how the liquid influences the submerged oscillator, and it is dynamically influenced by its shape, size, velocity, and fluid properties. Stokes' Law is a commonly employed equation for describing the drag force (F_d) experienced by objects moving at low to moderate speeds through a fluid and is expressed as

$$Fd = \frac{1}{2} C_d A_p \rho_l \dot{u}^2 \tag{27}$$

where C_d is the drag coefficient, A_p denotes the dragging object projected cross-sectional area perpendicular to the direction of flow, $\dot{u}$ is proportional to the velocity of the object, and ρ_l the fluid viscosity. The condensed form of the equation of motion follows Eq. (25) for its multiple-DOFs features, which, in this case, the local resonators assume three-DOFs.

4. Numerical analysis of the resonators

In Sharma et al. (2019), the authors presented the TSD analytical formulation and its experimental validation. Their parameters were assumed in our TSD model for validation purposes. Thus, the cylindrical tank has a radius of 0.2 m and is made of stainless steel. It is filled with water with levels varying from 0.2–0.5 m in steps of 0.1 m. The first fundamental lateral natural frequency is calculated and listed in Table 1. The TSD controls assume two analytical formulations, hydrodynamic (TSD1) and equivalent mechanical model (TSD2), detailed in Section 3.2. The results of our numerical model closely match those found in Sharma et al. (2019), indicating the accuracy of our TSD and multiphysic (hybrid) numerical model implementation.

Table 1
Comparison of the achieved first natural frequency (ω_1) of their slosh-based resonators within the work presented in Sharma et al. (2019).

Height - h [m]	ω_1[Hz] TSD1 (Sharma et al., 2019)	ω_1 [Hz] TSD1	ω_1 [Hz] TSD2	ω_1 [Hz] Hybrid
0.1	–	1.2906	1.288	1.29
0.2	1.47	1.4771	1.476	1.47
0.3	1.51	1.5087	1.508	1.51
0.4	1.51	1.5138	1.513	1.51
0.5	1.51	1.5146	1.514	1.51

This study validates the formulated resonators that are now designed to match some critical mode shapes of the OWT. For this application, the controllers are specifically engineered to mitigate the first and second resonant frequency of the NREL 5MW OTW (Jonkman et al., 2009). Further, the following analyses focus on the performance of the resonators in vibration mitigation of the desired frequency. Dynamic responses in frequency, time domain, and phase plane diagrams of the structural response are explored for each controller. These controllers include the undamped TMD, as shown in Figs. 6(a)–6(d), and TMD with additional hysteretic damping incorporated into its stiffness, shown in Figs. 6(e)–6(h). The hydrodynamic TSD is explored in Figs. 6(i)–6(l), the equivalent mechanical models of TSD, as seen in Figs. 6(m)–6(p), and the hybrid tuned dampers, presented in Figs. 6(q)–6(t).

The TMD control system comprises a single-degree-of-freedom (DOF) mass–spring-damping system, as discussed in Section 3.1. The mass ratio is assumed to be 10% of the OWT mass divided by the number of resonators, set at 13 for this analysis. A hysteric damping factor of $\zeta = 0.01$ is applied to the resonator's spring, and a unitary force is assumed in all cases. The designed controls operate at tuned resonant frequencies of 0.27 Hz, targeting the OWT's first resonant frequency. Receptance responses of both undamped and damped TMD are shown in Figs. 6(b) and 6(f), respectively, with a single resonant peak observed

Table 2
Liquid properties assumed in the TSD and hybrid resonators (Munson et al., 1995; Ocak et al., 2022).

Liquid	Dynamic Viscosity (Pa.s)	Temperature (°C)	Kinematic Viscosity (m^2/s)	Density (kg/m^3)
Acetone	0.306×10^{-3}	25	3.90×10^{-7}	784.89
Chloroform	0.58×10^{-3}	20	3.92×10^{-7}	1480.3
Mercury	1.57×10^{-3}	20	1.15×10^{-7}	13,600
Oil SAE15W40	287.26×10^{-3}	20	327×10^{-6}	872.5
Propanol	1.945×10^{-3}	25	2.43×10^{-6}	799.60
Sea water	1.20×10^{-3}	15.6	1.17×10^{-6}	1030

at the tuned frequency. Temporal responses for the TMD are shown in Figs. 6(c) and 6(g), where the decay in the damped system's response over time is due to damping. Fig. 6(d) and 6(h) illustrate trajectory curves of the structural response $\dot{u}$ by u for both TMDs, indicating stable and harmonic responses at this level of external excitation amplitude. The trajectory curves converge to a limit cycle, where for the damped TMD, the curve radius is decreased after excitation's initiation due to the structural damping. The trajectory curve indicates the structure's response is stable and harmonic at this external excitation amplitude level.

In all cases, TSD controllers assume a cylindrical tank with a radius set to 1.5 m, and the liquid height is calculated as $h = M_0/(\pi Rt^2 \rho_l)$ (Sharma et al., 2019). The hydrodynamic TSD assumes a single-DOF configuration with mass–spring-damping associated with the slosh component. Meanwhile, the equivalent mechanical TSD model consists of a two-DOF system represented by the active and passive tank liquid, which assumes seawater in this analysis. Receptance responses of TSD1 and TSD2 are displayed in Figs. 6(j) and 6(n), showing single and multiple resonant peaks at 0.27 Hz and 2.38 Hz, respectively, corresponding to the single and multiple DOFs of the dynamic controls. Both TSD controls' temporal responses, presented in Figs. 6(k) and 6(o), demonstrate decaying over time due to associated damping. Figs. 6(l) and 6(p) exhibit trajectory curves of the structural response for both TSDs, indicating stability in the system response as the curves converge to a limit cycle after excitation initiation, with the curve radius decreasing due to structural damping.

The multiphysics control (hybrid) integrates TSD with TMD completed as shown in Fig. 6(q) and employs a three-DOF system representing the active liquid tuned at 2.38 Hz, passive tank-liquid tuned at 10 Hz, and the TMD resonator operating at 0.27 Hz, as detailed in Section 3.3. Receptance responses of the hybrid resonator are shown in Fig. 6(r), with three first resonant frequencies set at tuned frequencies in line with the multiple DOFs of the dynamic controls. Fig. 6(s) illustrates the temporal response of the hybrid resonator, which decays over time due to associated damping, while Fig. 6(t) displays trajectory curves of the structural response, indicating stability as they converge to a limit cycle, with decreasing radius associated with damping. Compared to the TMD, TSD1, and TSD2 controllers, the hybrid resonator achieves more significant decaying in both temporal and trajectory curve responses while maintaining dynamic stability.

Various liquids can be used inside the TSDs, including acetone, mercury, seawater, chloroform, propanol, and oil SAE15W40, chosen for their suitable densities and viscosities, also commonly employed in fields like healthcare and the chemical industry. The properties of each liquid used in the analysis, such as density (ρ_l) and dynamic viscosity (v), acquired at constant temperature, are listed in Table 2.

Fig. 7 illustrates the receptance and temporal responses of the TSDs and hybrid controllers. These results explore the sensitivity of each liquid associated with the slosh-tuned damper. In Figs. 7(a–c), the receptance response, a zoom on the tuned frequency, and temporal responses, respectively, of the single-DOF slosh resonator (TSD1) modelled by the hydrodynamic theory are represented. The resonant peak's amplitude is highest for acetone, followed by chloroform, seawater, propanol, mercury, and oil SAE15W40. The temporal responses confirm this decreasing amplitude trend as a function of the liquid used, where the curves exhibit reduced amplitude over time. All liquids exhibit a damping effect, with Oil SAE15W40 presenting the best damping performance, followed by mercury, seawater, propanol, chloroform, and acetone.

Figs. 7(d–f) show the receptance response, a zoom on the tuned frequency, and temporal responses, respectively, of the two-DOF slosh resonator (TSD2) modelled by the equivalent mechanical theory. Two resonance peaks are observed at 0.27 Hz and around 2.38 Hz, corresponding to the active liquid of the slosh and the tank-passive liquid, respectively. This controller is designed to match the shapes of the first and second wind turbine modes. The amplitude of the resonant peak is highest for chloroform, followed by acetone and seawater, propanol, mercury, and oil SAE15W40. This change in amplitude, compared with the hydrodynamic theory, is due to the contribution of a second-mode shape, which induces a slight reduction and modification in the first mode. Both numerical models exhibit similar dynamic behaviours associated with the liquid choice. As the temporal response shows, the highest amplitude is inversely proportional to the curve decay over time. Hence, Oil SAE15W40 exhibits the best damping performance, followed by mercury, propanol, seawater, acetone, and chloroform. Therefore, all liquids exhibit a damping effect in the resonator's dynamic response.

The receptance and temporal responses of the three-DOF hybrid resonator are shown in Fig. 7(g–i). The equivalent mechanical model of this resonator consists of three DOFs related to the TMD oscillator, active slosh liquid, and the tank-passive liquid, tuned at 0.27 Hz, 2.38 Hz, and 10 Hz, respectively. The oscillator exchanges energy with the liquid inside the tank through resonance alongside the interaction with the liquid as it sloshes due to container vibration, thus creating a complex fluid–structure interaction, contributing to the overall vibration reduction mechanism. The oscillator operates in parallel with the active slosh, and the liquid opposes its oscillation through drag force, influencing the damping coefficient. Fig. 7(h) displays a zoom of the receptance response at the first resonant peak related to the oscillator operational frequency. The amplitude curve is highest for mercury, while the other liquids exhibit close amplitudes with slight differences in the resonant peak, followed by chloroform, seawater, oil SAE15W40, propanol, and acetone. Temporal responses show mercury with a higher amplitude but good decay over time. The other liquids display close amplitudes and greater damping over time. Among the tested liquids, oil SAE15W40 demonstrates the best performance in adding damping to the system.

5. Numerical results of the metamaterial wind turbine

The 5MW monopile OWT's first and second vibration modes amplitude is targeted to be attenuated using TMD, slosh and hybrid multiphysics metamaterial turbine. The design based on TMD resonators demonstrated that distributing the resonators along the turbine provides a more effective configuration, as demonstrated in Machado et al. (2024). Aside from the optimal metamaterial configuration, the authors demonstrated the attenuation band. Hence, based on this preview study, the resonators are assumed to be periodically placed along the wind turbine's tower in all cases, as shown in Fig. 8(b). Further, the turbine metamaterial using slosh and hybrid resonators is compared

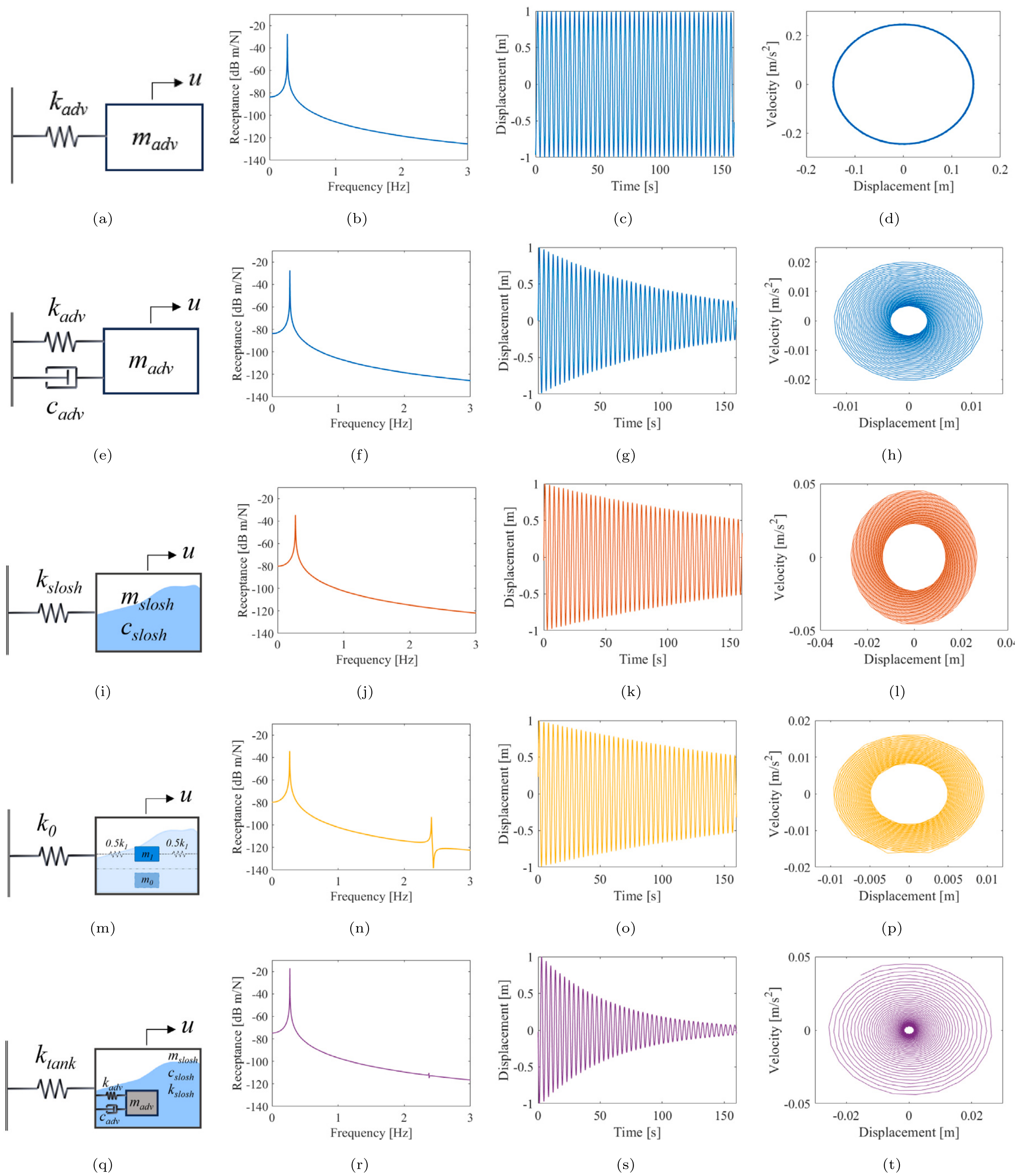

Fig. 6. Resonator representation, receptance response, temporal, and phase diagram responses, respectively for: (a–d) undamped TMD, (e–f) TMD with hysteretic damping of 0.01 of damping factor, (i–l) TDS1, (m–p) TSD2, and (q–t) Hybrid resonator.

with the TMD resonator type. The resonator configurations align with the analysis shown in Figs. 6–7. A hysteretic damping factor of $\zeta = 0.01$ is applied to the resonator's spring attached to the turbine tower wall, and the performance of each resonator in mitigating vibrations of the metamaterial turbine under unitary force and various hazard forces was investigated. The metamaterial NREL 5 MW offshore wind turbine, featuring a monopile foundation and three-bladed horizontal axis virtual turbine (Jonkman et al., 2009; Jonkman and Musial, 2010). This turbine's properties are well-documented in the existing literature and are described in Table 3. With a tower height of 87.6 m above water level and a hollow monopile foundation length of 20 m (measured between mean sea level and ground level), the buried monopile length in the soil ranges from 30 to 45 m (Jonkman et al., 2009). Therefore, this study assumes the pile is fully fixed at ground level and has no soil–structure interaction to seek to simplify the metamaterial design.

The excitation force, with a unitary magnitude, is applied at the free end (interface point-10), and the receptance responses are estimated along the turbine tower's interface, guided by points 0 to 10 in Fig. 8(a). The vibration characteristics of the uncontrolled NREL 5 MW OWT monopile are presented in Fig. 8. The validation of the spectral and the metamaterial OWT (with a TMD controller assumed in its construction) is conducted with the FEM model given in supplementary material following Ref. Machado et al. (2024). Hence, the OWT and TMD metamaterial turbine is assumed as a reference model and used to validate the slosh and multiphysics metamaterial turbine proposed

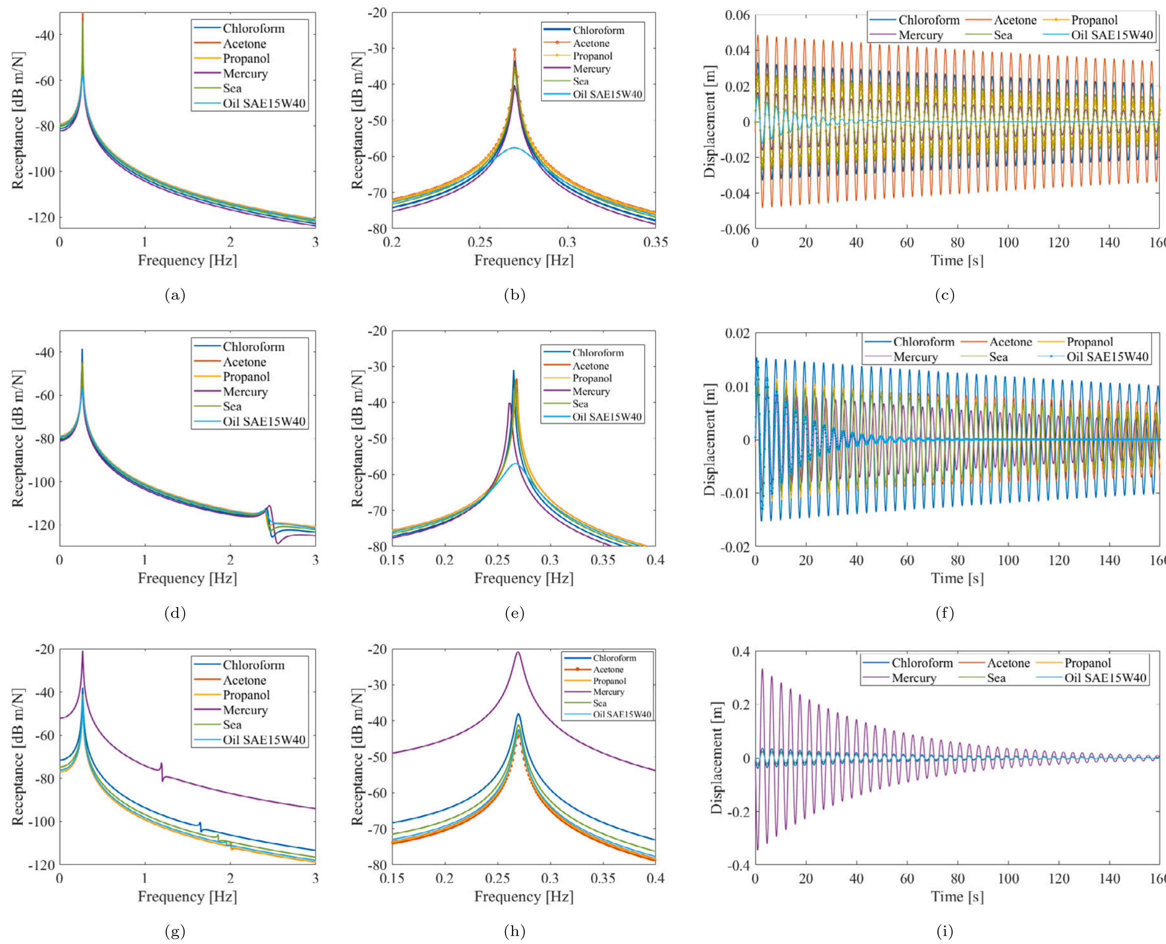

Fig. 7. Receptance response, zoom at first resonant peak, and temporal response of the liquid resonators for different liquids (acetone, chloroform, mercury, oil SAE15W40, propanol, seawater). (a–c) TSD1, (d–f) TSD2, and (g–i) Hybrid resonators.

Table 3
NREL 5 MW offshore wind turbine parameters (Jonkman et al., 2009).

Wind turbine properties	Value	Wind turbine properties	Value
Max rater power	5 MW	Rotor diameter	126 m
Tower heigth	87.6 m	Hub diameter	3 m
Rotor hub height	90 m	Tower top section diameter	3.87 m
Monopile height	20 m	Tower bottom diameter	6 m
Tower mass	347,460 kg	Tower wall thickness	27–19 mm
Rotor mass (with hub)	110,000 kg	Monopile wall thickness	27 mm
Nacelle mass	240,00 Kg	Nacelle inertia - Yaw axis	2,607,890 kg m^2
Rated speed (Cut-In)	6.9–12.1 rpm	Hub inertia - Low speed	115,926 kg m^2

in this paper. All designed controls operate at the turbine's first and second resonant frequencies, 0.27 Hz and 2.38 Hz, respectively. The total mass ratio varies from 5% to 20%, covering a range of mass ratios and quantities of resonators.

Figs. 8(c) and 8(d) display the temporal and receptance responses of the uncontrolled OWT obtained at point 10 of the interface, and Fig. 8(e) illustrates the receptance response heatmap over its interface, with red and yellow lines marking the highest amplitudes of each mode's resonance peak. Meanwhile, the bluish area represents anti-resonance and lower amplitudes of the spectrum. Fig. 8(f) presents the spectrogram of the inertance response of the wind turbine under unitary excitations across the entire frequency band. The power level for the first resonant frequency range is visible for up to 2 min, and similarly for the second resonance. All spectrograms are calculated using the spectrum-Matlab function, assuming a frequency resolution of Fres = 42.807 mHz and a time resolution of Tres = 59.9609 s, with the frequency and temporal acceleration response as input. It illustrates how the frequency power content in the signal changes over time. The first resonant mode exhibits a higher amplitude in the analysed frequency band, enhanced by the force excitation. Consequently, the signal power is prominent at lower frequencies, and due to structural damping, it gradually decreases in amplitude over time.

5.1. Vibration attenuation with metamaterial OWT under unitary excitation

All cases presented in this section assume that the temporal and receptance responses are calculated at the top of the turbine, where a higher displacement amplitude is reached in the first mode. The receptance heatmap is along the turbine's length, and the spectrograms compare the uncontrolled turbine with the controlled turbine, with a mass ratio ranging from 5% to 20% are given in the supplementary material, Appendix. Fig. 9(a–d) illustrates the performance of the metamaterial turbine assuming the TMD resonator controller. The receptance response of the turbine, shown in Fig. 9(b), primarily

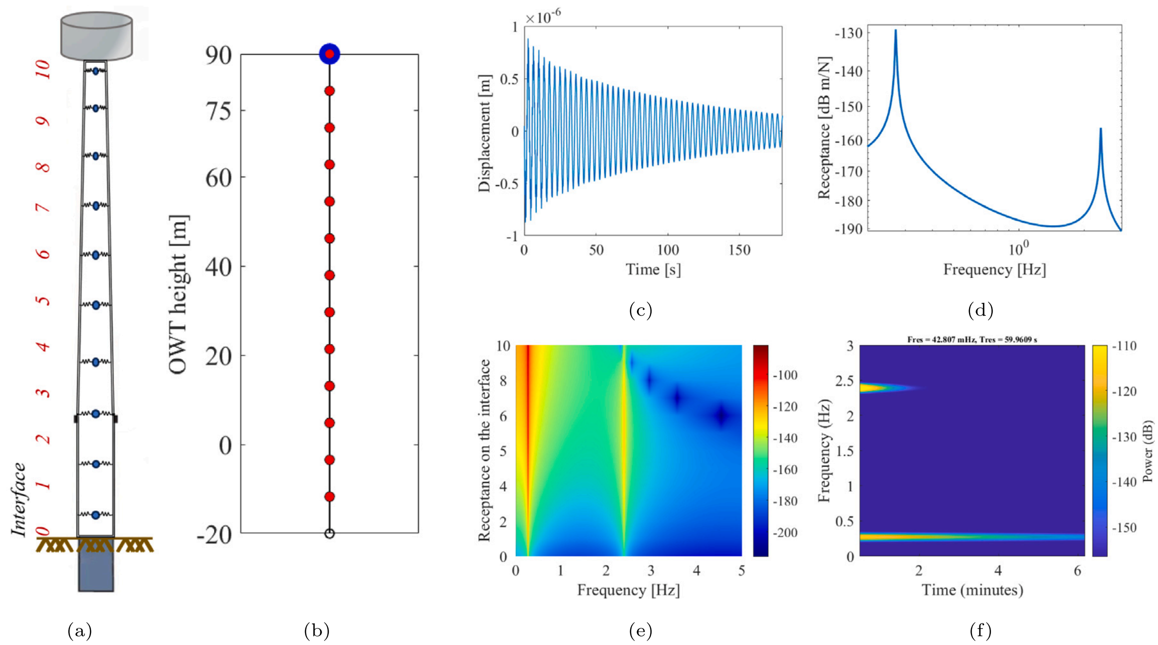

Fig. 8. Simplified wind turbine metamaterial (a). Schematic spectral modelling representation with red dots representing the attached resonators (b), where coordinate zero in the y-axis marks the MSL. Uncontrolled OWT's responses: (c) temporal, (d) receptance response, (e) Heatmap receptance response obtained on the interface, and (f) the spectrogram of the OWT inertance response. (For interpretation of the references to colour in this figure legend, the reader is referred to the web version of this article.)

influences the first frequency control while leaving other mode shapes unaffected. The TMD single-DOF resonator typically operates within a narrow frequency range. This passive vibration control method has a well-defined working range. Still, if operated outside this range, it may lead to undesirable behaviour, such as a creation or increase in the amplitude of adjacent modes. The locally resonant bandgap targets the modal neighbourhood and appears when an infinite number of resonators are placed on the structure. By incorporating the TMD resonator in the metamaterial turbine design, a shift in the target resonant peaks is observed, accompanied by a decrease in amplitude of 5 dB. Additionally, the width of the open attenuation gap increases with the mass ratio.

Fig. 9(c) presents the receptance response heatmap of the controlled OWT across its interface. In the heatmap, red marks indicate the highest amplitudes of each mode's resonance peak, while the bluish area represents anti-resonance and lower amplitudes. The turbine exhibits structural damping, evidenced by the decrease in the blue curve temporal displacement. With the addition of the controller, the temporal curve in Fig. 9(a) the waveforms show the independent amplitude and signal frequency modulation due to the two resonant frequencies induced by the split of the target mode shape. The amplitude decreases over time because of the structural damping, and a slightly reduced amplitude is related to the mass ratio. Figs. 9(d) display the spectrogram of the inertance response of the wind turbine under unitary excitation across the frequency range 0 to 1 Hz and mass ratio of 20%. The spectrogram illustrates how the frequency power content in the signal changes over time, with yellow representing higher amplitudes and blue lower ones. The first resonant mode exhibits higher amplitude in the analysed frequency band, enhanced by the force excitation. The signal power is prominent in lower frequencies and, as in the time and frequency spectra, gradually decreasing amplitude over time due to structural damping. The efficacy of the control is determined by the reduction of the yellow area on the spectrogram, indicating a decrease in overall power levels in the signal and, consequently, vibration amplitude. The yellowish region highlights the power levels of the signal.

The performance of the metamaterial turbine with TSD resonator controller formulated using hydrodynamic theory adopted by the metamaterial, with seawater assumed as the fluid inside the tank, is shown in Fig. 9(e–h). TSD1 works as a one-DOF system and functions within a single frequency, specifically chosen for each of the first OWT mode shapes. Fig. 9(f) displays the receptance response of the turbine adapting to the TSD1 dynamic behaviour, primarily influencing the first frequency control. Similar to TMD, TSD1 operates within a narrow frequency range. A shift in the target resonant peaks is observed, accompanied by a 5 dB decrease in amplitude. Additionally, the width of the open gap increases with the mass ratio. Fig. 9(g) presents the receptance response heatmap of the controlled OWT across its interface, with red marks indicating the highest amplitudes of each mode's resonance peak and the bluish area representing anti-resonance and lower amplitudes. The temporal curve in Fig. 9(e) exhibits the emergence of two new frequencies by the pulse shape over time, maintaining decay for all mass ratios due to turbine structural damping. Consequently, in some time frames, the amplitude increases compared to the uncontrolled turbine response, indicating that TSD1 follows TMD without imposing a significant change in displacement reduction. Figs. 9(h) display the spectrogram of the inertance response of the wind turbine under unitary excitation across the frequency band range from 0 to 1 Hz and for a mass ratio of 20%. The first resonant mode exhibits higher amplitude in the analysed frequency band, enhanced by the force excitation. Consequently, the signal power is prominent in lower frequencies, gradually decreasing amplitude over time due to structural damping.

Figs. 9(i–l) show the results of the metamaterial turbine composed by the TSD resonator controller formulated with the two-DOF equivalent mechanical theory with seawater adopted as the fluid. In this case, the TSD2 operating frequencies are 0.27 and 2.38 Hz. The receptance response of the turbine, shown in Fig. 9(j), captures the two local resonant gaps controlling both frequencies. The first frequency exhibits a similar broadband gap size split as in the TSD1 case, performed by the slosh-DOF, while the second frequency is governed by the tank/passive liquid-DOF. Both frequencies shift in the target resonant peaks, and

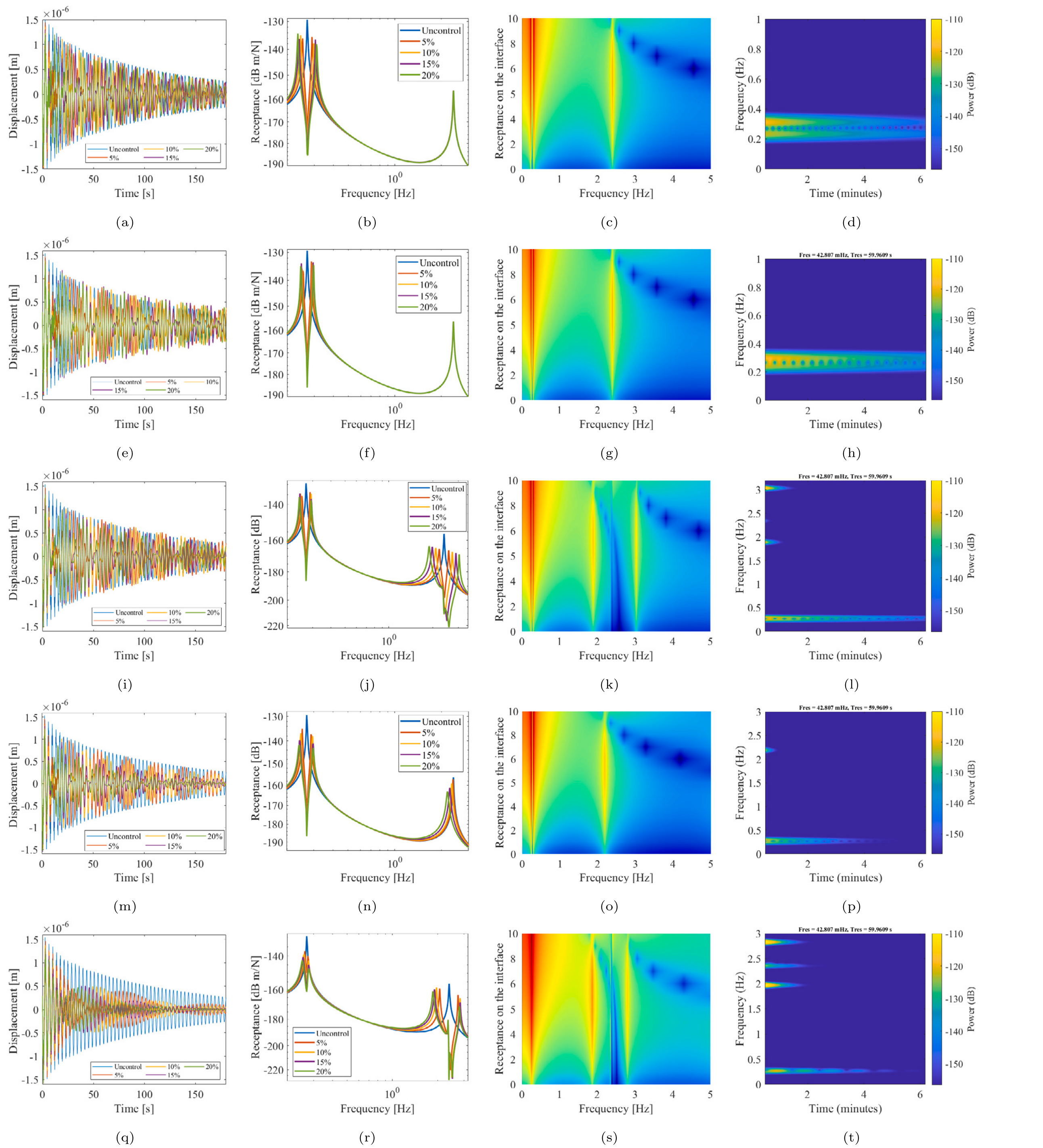

Fig. 9. Metamaterial OWT's temporal and frequency responses target the first and second mode shape with ϵ = 5 to 20%. The heatmap and spectrogram assume ϵ = 20%, for other ϵ values, see Appendix. The resonator types are (a–d) TMD, (e–h) TSD1, (i–l) TSD2, (m–p) Hybrid-w1w1, and (q–t) Hybrid-w1w2. (For interpretation of the references to colour in this figure legend, the reader is referred to the web version of this article.)

the open attenuation gap increases with the mass ratio. The resonant amplitude reduction is about 5–7 dB on the first mode and 10–12 dB on the second mode, depending on the mass ratio. The receptance response heatmap of the meta-turbine coupled with TSD2 is shown in Fig. 9(k), where the red marked lines indicate the highest amplitudes of the first mode. At the same time, the bluish area represents anti-resonance and lower amplitudes. A distinct shifting resonance frequency effect is also observable as a horizontal yellow line traversing the heatmap. This line indicates the second resonant frequency split. A bluish zone is visible in this open gap mode, which is the local bandgap effect.

The meta-turbine's temporal curve in Fig. 9(e) follows the decay over time due to the turbine's structural damping. No decrease in amplitude compared to the uncontrolled system is observed, only the change in the resonant frequency of the turbine is due to the splitting resonances effect of the added metamaterial control. The temporal response by the signal modulation over time observes the composition of multiple near-resonating peaks. Fig. 9(l) shows the spectrogram of the metamaterial turbine composed of TSD2 resonators across the frequency band of 0 to 3 Hz and for ϵ of 20%. The first and second resonant modes exhibit higher amplitudes in the analysed frequency bands. The

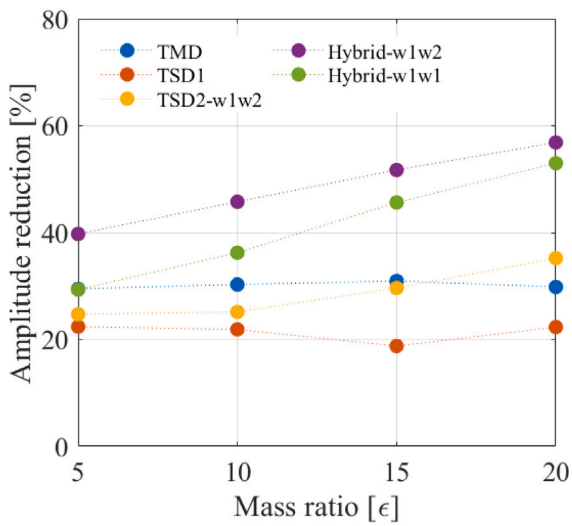

Fig. 10. Amplitude reduction level achieved by the metamaterial turbine with the mass ratio of 5, 10, 15 and 20%.

Table 4
Mass of each resonator(mass ratio) associated with the number of resonators considered for each configuration used to control the first, second, and first–second resonant frequencies.

Number of resonator	Mass ratio[ϵ in %] - Mass of each resonator [Kg]				
	$\epsilon = 1$	$\epsilon = 5$	$\epsilon = 10$	$\epsilon = 15$	$\epsilon = 20$
1	6.975	34.873	69.746	10.4619	13.9492
7	996	4.982	9.964	14.946	19.928
13	537	2.683	5.365	8.048	10.730
26	258	1.341	2.683	4.024	5.365

mass ratio effect is more prominent in the second mode, where the open gap induced by the controller enlarges with the mass increase. Signal power is prominent in lower frequencies and gradually decreases amplitude over time due to structural damping. Fig. 9(m–t) presents the results of the metamaterial turbine assuming hybrid control resonators formulated based on the three-DOF equivalent mechanical mode theory with seawater adopted a filling liquid, with operating frequencies in two configurations: Hybrid-w1w1, where the oscillator operates at 0.27 Hz, the slosh at 2.38 Hz, and the tank/passive liquid at 10 Hz (Fig. 9m–p), and Hybrid-w1w2, with the oscillator and slosh operating at 0.27 Hz and the tank/passive liquid at 10 Hz (Fig. 9q–t). The receptance response of the turbine, shown in Fig. 9(n), captures the local resonant gap around the first mode and amplitude reduction on the second mode by 5–8 dB depending on the mass ratio. The split of the first mode, combined with amplitude reduction of the adjacent peaks, varies from 5–12 dB relative to the mass ratio. Fig. 9(o) shows the receptance response heatmap, indicating control on the first mode by the red shade lines. The temporal curve in Fig. 9(m) of the meta turbine follows the decay over time due to the turbine structural damping. A decrease in amplitude compared to the uncontrolled system is observed. A reduction in the amplitude of the curve follows the increase in the mass ratio, with the 20% mass ratio presenting the highest amplitude reduction, which is enforced by the spectrogram in Fig. 9(p). The power remains in the meta turbine for both, presenting the best reduction in time for the $\epsilon = 20\%$ followed by 10%.

By tuning the oscillator to 0.27 Hz and the slosh to 2.38 Hz, one can control the shape of the turbine in the first two modes. Fig. 9(r) shows the metamaterial turbine's receptance response, capturing the local resonant attenuation gaps around the first and second modes with amplitudes reduced by 8–12 dB and 4–5 dB, respectively, depending on the mass ratio. In both mode shapes, the split of the resonance mode is combined with amplitude reduction. Fig. 9(s) shows the receptance response heatmap, indicating control on both resonant peaks, highlighted by red marked lines for the first mode and yellow-orange lines for the second mode. The metamaterial turbine's temporal curve in Fig. 9(q) follows the decay over time due to the turbine structural damping but also shows reduced displacement amplitude compared to the uncontrolled system. The amplitude reduction of the curve follows the increase in mass ratio, with the 20% mass ratio presenting the highest amplitude reduction. Fig. 9(t) shows the spectrogram in the frequency band of 0 to 3 Hz and for ϵ of 20%, respectively, where the first resonant frequency experiences drastic amplitude attenuation over time, with significant decay. The second resonant mode exhibits adjacent modes due to the target frequency split and an additional spectrum representing some internal attenuation band local mode (Machado and Dutkiewicz, 2024a). Overall, the power amplitude related to this mode decays rapidly over time. The power remains in the meta turbine, with the best reduction over time observed for the $\epsilon = 20\%$.

Overall, the TMD, TSD1, and TSD2 locally control the frequency by preventing significant signal amplitude decrements, mainly influenced by the turbine's structural damping. Therefore, the shift of the target resonance exists at local frequencies, demonstrating the efficacy of TMD and TSD local vibration control. The hybrid-tuned damper resonator solution shows better attenuation based on both temporal and frequency responses, with Hybrid-w1w2 exhibiting the best performance. The quantification and evaluation of vibration reduction achieved in each metamaterial OWT design's performance are defined by the time signal's root mean square (RMS) value. RMS measures the waveform's amplitude and provides a value directly correlated with the energy content, making it a suitable metric for quantifying vibration control efficiency. The percentage of vibration attenuation achieved by each control system is estimated using the response amplitude reduction, $AMP_r = 100 * \left[(RMS_{un} - RMS_{mc})/RMS_{un}\right]$, where RMS_{un} is the time signal RMS value for the uncontrolled turbine and RMS_{mc} time signal RMS value for the metamaterial OWT. Fig. 10 show the graphic of the amplitude attenuation level achieved by each metamaterial turbine design, considering mass ratio varying from 5 to 20%. The resonators TMD, TSD1, and Hybrid-w1w1 control only the fist resonance mode shape, with Hybrid-w1w1 showing the best performance among the resonators, achieving 30%–52% in displacement amplitude reduction with a 5%–20% mass ratio, followed by the TMD achieving 28%–29%, and TSD1 with 18%–22% in displacement amplitude reduction. The resonators TSD2 and Hybrid-w1w2 perform simultaneous control at the first and second resonate peaks, where the Hybrid-w1w2 best promoted the displacement reduction, achieving 40%–58% in amplitude reduction, followed by the TSD2 that achieved 24%–35% in amplitude reduction.

The design of the resonator's dynamic properties is intrinsically linked to the mass ratio and the desired target frequencies for control. Ranging from 5 to 20% of the turbine mass, the mass ratio encompasses both first- and second-mode shapes requiring control. In Table 4, the mass values of each resonator are detailed and associated with the finite number of resonators assumed in the metamaterial OWT design. Classical TMD control, where only an oscillator controls the turbine, demands the highest stiffness, mass, optimal inflation point, and significant mass value. However, embracing the metamaterial design reduces the resonator's mass and stiffness while maintaining or enhancing the vibration control effects. Table 4 compares the finite number of resonators in the metaturbine turbine with the resonator's mass. The case of 1 TMD defines the classic single control, and multiples resonators (7, 13, and 26) is the case of the metamaterial. A significant reduction in the resonator's size and mass is demonstrated, combined with an improvement in the attenuation response level. While the ideal number of resonators used in the metamaterial is infinite, this number can be treated as a design requirement for practical purposes. The outcome of

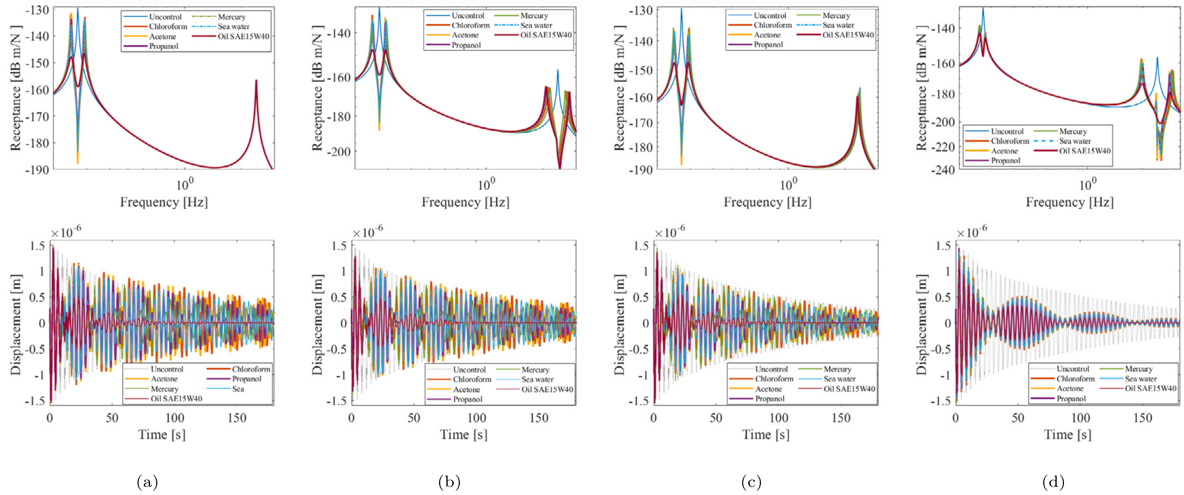

Fig. 11. Receptance and temporal responses of the meta turbine designed with the tuned slosh damped control contain different liquids such as chloroform, acetone, propanol, seawater, and oil SAE15W40. The TSD formulation and mass ratio of 10% are displayed as: (a) TSD1, (b) TSD2, (c) Hybrid-w1w1, and (d) Hybrid-w1w2.

the metamaterial design demonstrates a decrease in stiffness values as the number of resonators increases, consequently reducing the size and weight of the control device. Besides bandwidth control, the design of resonators plays a pivotal role in the overall control strategy, especially concerning manufacturing and installation. In contrast to conventional TMD control, the wind turbine metamaterial offers a combination of wide operational bandwidth and frequency attenuation, achieved with reduced stiffness and resonator size.

5.1.1. Enhancing vibration control efficiency with slosh and multiphysics resonators

The TSD and hybrid resonator systems initially assume seawater as the liquid in the intake. Therefore, various commercial liquids are utilised for this purpose. Fig. 11 investigate the efficacy of acetone, mercury, seawater, chloroform, propanol, and oil SAE5W40 as control liquids, with their properties detailed in Table 2. The liquid's influence on the resonators' dynamic responses is illustrated in Fig. 7, where characteristics such as liquid properties, sloshing energy, damping rate, and period are examined. Consequently, the density and kinematic viscosity of the selected liquid play crucial roles in modulating the damping effect performed by the resonators, which can be fine-tuned through adjustments in spring stiffness and liquid mass. The total liquid mass of the tank and the spring stiffness are contingent upon factors such as liquid density, tank geometry, and the damping rate parameter, which is influenced by the liquid's kinematic viscosity. Thus, the choice of liquid employed in the TSD significantly impacts the response of the primary structure, notably the wind turbine. The higher the mass ratio, the better the vibration attenuation effect. However, adding mass to the system may lead to structural issues; as a compromise, further analysis assumes $\epsilon = 10\%$.

Fig. 11(a–b) presents the receptance and temporal responses of the meta turbine designed with tuned slosh damper control, utilising different liquids such as chloroform, acetone, propanol, seawater, and oil SAE15W40, where Fig. 11(a) display the responses of TSD1 for mass ratio of 10% and Fig. 11(b) illustrate the responses of TDS2. Through dynamic interaction, the TSD absorbs some of the mechanical energy the primary structure receives from the environment, inducing motion to the filled tank liquid. Generally, the energy dissipation mechanism of the TSD arises from one or a combination of three phenomena comprehending liquid sloshing (with or without wave breaking), liquid movement through orifices, and relative motion between the liquid and submerged objects. In the cases of TSD1 and TSD2, the dissipation is primarily attributed to liquid sloshing phenomena, whereas lower kinematic viscosity causes better performance of the controller. Among the top three liquids, acetone and chloroform exhibit nearly identical kinematic viscosities, with chloroform being twice as dense as acetone. Hence, the less dense liquid tends to yield closer to the optimal result in liquids with similar kinematic viscosity properties. When comparing the resonator efficiency based on density, mercury, ten times denser than other liquids, had a close performance of the others, indicating that density alone cannot be a decisive criterion for the control damping efficiency, and liquid viscosity plays a more significant role. Oil SAE15W40, characterised by higher viscosity and lower density, demonstrates the most effective damping effect among the liquids.

Fig. 11 (c-d) displays the receptance and temporal responses of the meta turbine designed with hybrid resonator control, filled with chloroform, acetone, propanol, seawater, and oil SAE15W40. Figs. 11(c) show the responses of resonators configured to operate at 0.27 and 10 Hz (Hybrid-w1w1), while Figs. 11(d) illustrate the hybrid resonator (Hybrid-w1w2) configured to operate at 0.27, 2.38, and 10 Hz, with mass ratio of 10%. The hybrid resonator combines the energy dissipation mechanism of slosh with the relative motion between the liquid and submerged oscillator, enhancing vibration amplitude reduction. In addition to the kinematic viscosity and density of the liquid, the drag force opposing the oscillator movement imposed by the liquid influences the damping coefficient associated with the resonator type. Oil SAE15W40 exhibits the most effective damping effect among the liquids, followed by propanol, acetone, seawater, chloroform, and mercury. By controlling the first and second mode shapes, the reduction in displacement amplitude imposed by the Hybrid-w1w2 resonator overreaches the Hybrid-w1w1 configuration due to the control of both turbine mode shapes. The results concerning the evaluation of mass ratio ranging from 5 to 20% for the TSD1, TSD2, and Hybrid are present in the supplementary material.

Fig. 12 illustrates the amplitude attenuation levels achieved by each design associated with different liquids. The control designs vary in mass ratio from 5 to 20%, and the attenuation performance of each resonator configuration is shown in Fig. 12. TSD1 and TSD2, shown in Fig. 12(a) and (b), respectively, exhibit attenuation ranging between 15%–38% for all liquids except oil, which outperforms 60%. Hybrid-w1w1 resonators show attenuation levels between 20%–61%, while Hybrid-w1w2 resonators demonstrate levels between 40%–68%, as shown in Fig. 12(c) and (d), respectively. Across all configurations, the highest reduction within the slosh dampers is achieved using Oil SAE15W40, with over 60% RMS amplitude attenuation. Amplitude reduction increases linearly with the mass ratio for all resonators. Propanol and acetone enhance the damping factor in hybrid resonators, indicating that lower-density fluids improve the damping

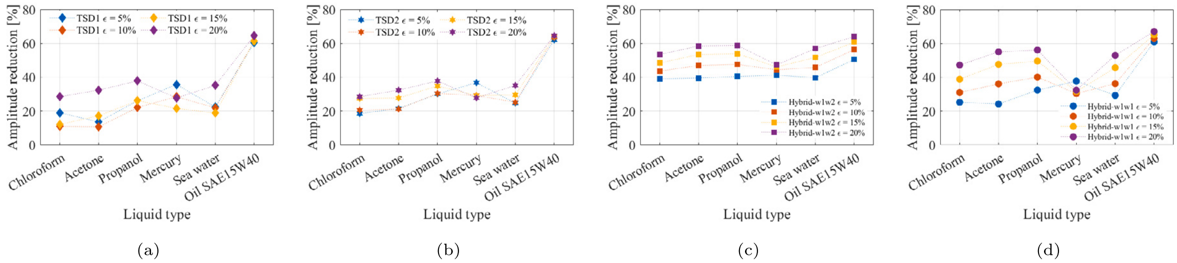

Fig. 12. RMS amplitude reduction level achieved by controllers TSD and hybrid for different liquids attached to the metamaterial turbine with the mass ratio of 5, 10, 15 and 20%.

effect, followed by seawater, chloroform, and mercury.

5.2. Vibration attenuation with metamaterial OWT under multiple hazards excitation forces

The multiple loads' power spectrum loads excitation modelled as described in Section 2.1, simulating blade rotation, wave, and the combined forces wind-wind-rotation are shown in Figs. 13(a) to 13(d), respectively. The combined PSD of the loads can be applied to all discretised nodes of the turbine model, as the responses are computed at these nodes. However, since our primary interest lies in the top node response, the multi-load PSD is specifically used to calculate the response at that location. A brief description of the theory used to model the loads is given in Appendix.

Fig. 13 compares the turbine dynamic auto-spectral density responses under unitary excitation, wind, waves, blade rotation, and combined loads. The receptance Frequency Response Function (FRF) of the OWT is calculated for unitary excitation, with well-defined mode shapes for both modes. Under wave excitation, the OWT auto-spectrum response exhibits a decrease in amplitude across the entire frequency range, along with an additional peak at 0.14 Hz corresponding to the JONSWAP wave sea surface elevation. Wind excitation, conversely, amplifies the amplitude of the first mode while reducing that of the second mode, attributed to the power density characteristic of the Kaimal spectrum. Blade rotation excitation amplifies the first resonant frequency and introduces significant resonance frequencies at 0.20 Hz, 0.4 Hz, and 0.6 Hz. Combining the multiple excitation, the first mode increases in amplitude, and new resonant peaks relate to the excitation frequencies. The PSD's loads exhibit high density at lower frequencies and decrease across the frequency band. This frequency content primarily excites the first or lower modes of the structure, inducing the contribution of higher-order modes to negligible or even modulating the structure responses. This modulation behaviour is evident in the frequency-domain response, where the resonance peaks for higher-order modes are considerably smaller in magnitude than those of the receptance responses.

Fig. 14 presents the auto-spectrum density and displacement of the metamaterial OWT comprising the frequency and time domain's first and second resonant frequency. Both responses are calculated at the top of the turbine and are excited by multiple forces, including wind, blade rotation, and waves. The control mass ratio is assumed to range from 5% to 20%, and the resonator designs considered are TMD, TSD1, TSD2, Hybrid-w1w1, and Hybrid-w1w2, shown in Figs. 14(a–e), respectively. The efficiency and pattern of multiple hazard vibration control in the meta-turbine follow the achieved response. Similar patterns were observed in the controllers of metamaterial turbines under unitary excitation, indicating that each resonator has its dynamic characteristics, which affect the metamaterial turbines' responses differently and are directly associated with the resonator rather than the excitation force. Seawater is the assumed liquid used to obtain these results. Fig. 14(f) illustrates the amplitude attenuation levels achieved by each metamaterial turbine design, with control designs varying in mass ratio from 5% to 20%. Resonators TMD, TSD1, and Hybrid-w1w1 control only the first resonance mode shape, with Hybrid-w1w1 exhibiting the best performance among the resonators, achieving 36% to 39% in displacement amplitude reduction associated with the mass ratio, followed by TSD1 achieving 34% to 9% in displacement amplitude reduction, and TMD achieving 28% to −8%, where negative values indicating amplification of displacement amplitude instead attenuation.

In this case, decreasing amplitude level control associated with the mass ratio is due to the slipt of the tuned resonant modes. Depending on their shift, the neighbouring frequencies coincide with the excitation frequencies, amplifying the amplitude. Resonators TSD2 and Hybrid-w1w2 simultaneously control the first and second resonant peaks. Hybrid-w1w2 achieved the best displacement reduction, with 42% to 58% amplitude reduction, followed by TSD2, which achieved 35% to 30% amplitude reduction. Overall, the hybrid controllers exhibited the best vibration control in displacement amplitude reduction. The results of the spectrograms of the metamaterial turbine designed with TMD, TSD1, TSD2, and Hybrid with 5 to 20% of mass ratios are given in the supplementary material, Appendix.

Fig. 15 demonstrate the vibration reduction capability of slosh-damped resonators when filled with different types of liquid, including chloroform, acetone, propanol, mercury, seawater, and oil SAE15W40. The analyses consider a mass ratio set at 10%, and Fig. 16 shows the percentage reduction level for mass ratios ranging from 5 to 20%. The spectrogram for the oil SAE15W40 case is presented in the analysis because it achieves the best performance in all cases, for the results achieved by the other liquids access the supplementary material, Appendix. Fig. 15(a–c) explores the TSD1 metamaterial turbine's auto-spectrum responses associated with the chosen liquid and its temporal and spectrogram responses. In contrast, Fig. 15(d–f) investigates specific liquids-related features which impose the control on first and second resonant frequencies. In both cases, the resonance modes exhibit a frequency shift accompanied by a reduction in amplitude, as clearly shown in the temporal and spectrogram graphics. Figs. 15(g–i), and 15(j–m) show the results in frequency, temporal and spectrogram for the hybrid resonators tuned at first and first–second turbines resonate frequencies. Those results highlight the effectiveness of slosh resonators and the potential improvement associated with the types of liquids used in control.

The amplitude reduction level achieved by controllers TSD and hybrid for different liquids designed for the metamaterial turbine with the mass ratio of 5, 10, 15 and 20% is demonstrated in Fig. 16. Hybrid resonators overreach the vibration reduction capability of slosh-damped-based resonators. The best-filled liquid shown to be the Oil SAE15W40, in all cases, presenting amplitude reduction of over 55%, followed by propanol, acetone, seawater, mercury, and chloroform. The outcomes provide a comprehensive analysis of the vibration reduction capability of slosh-damped based resonators even on the wind turbine under multiple hazard forces.

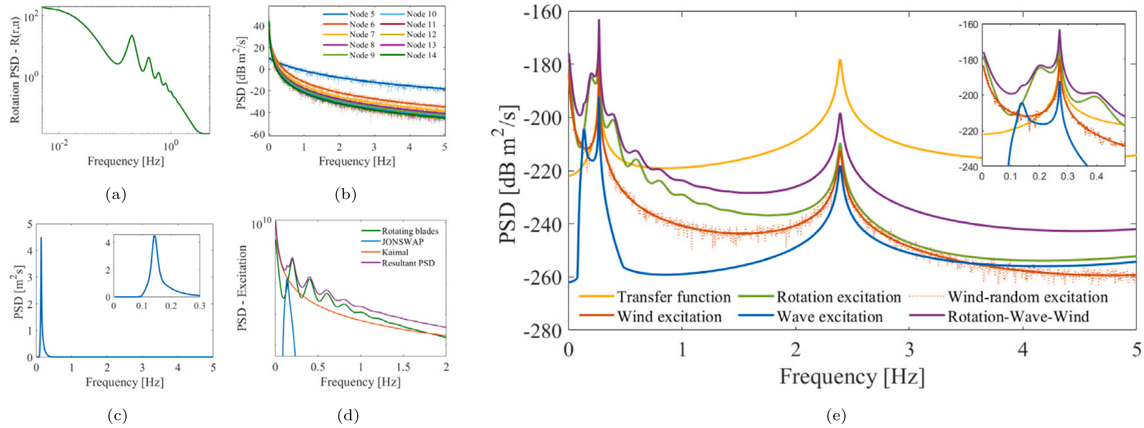

Fig. 13. External force power spectrum density simulating the (a) Blade rotation, (b) Kaimal along the turbine, (c) JONSWAP wave sea surface elevation, and (d) Combine wave-wind-rotation PDS. (e) Comparison for the OWT top receptance response for unitary excitation (Transfer function - yellow line), PSD for wave excitation (blue line), PSD for wind excitation (orange line), PSD for wind excitation (orange line), PSD for blade rotation excitation (green line), PSD for the resultant combination of all excitation (purple line).

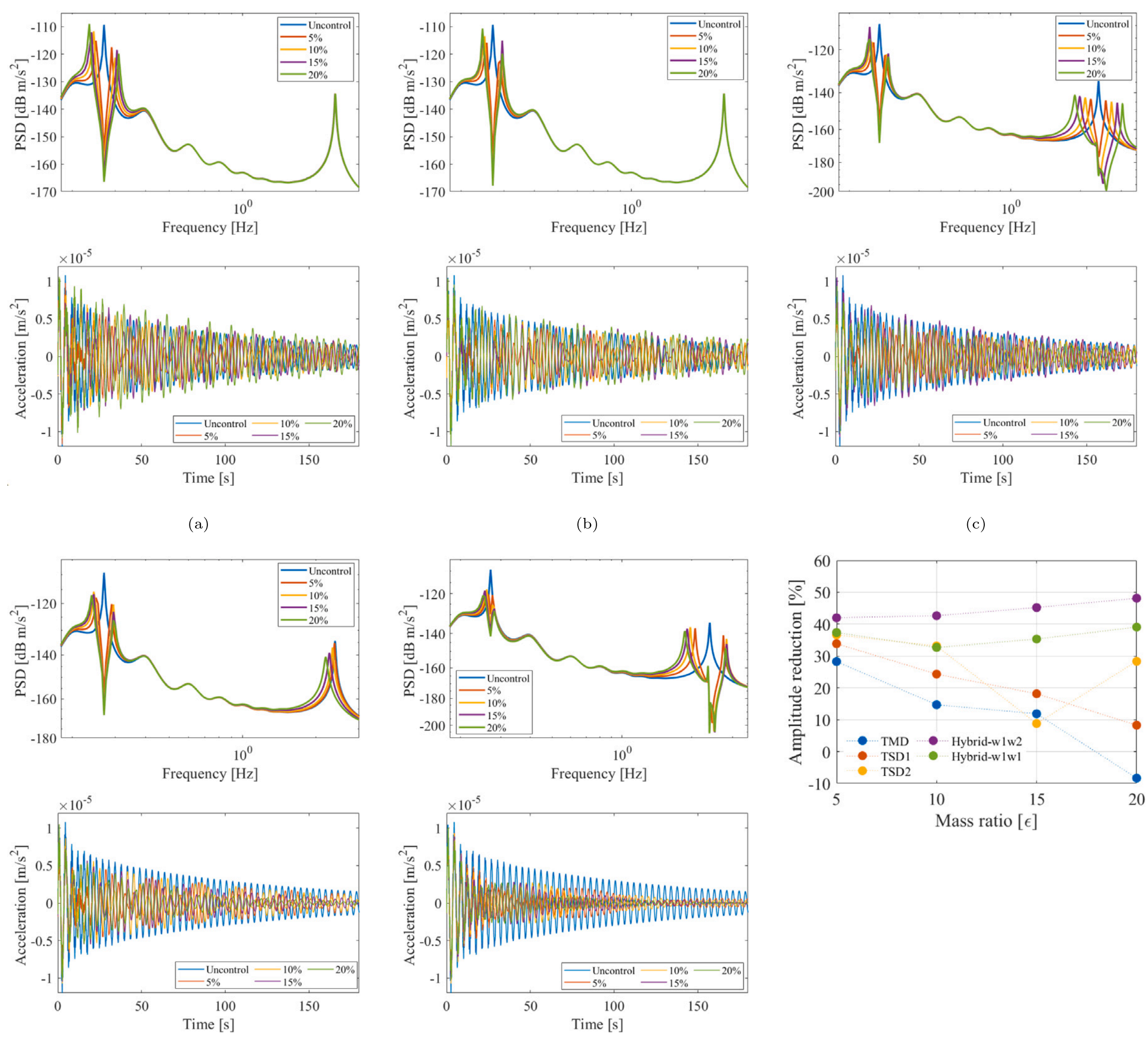

Fig. 14. Inertance and temporal auto-spectrum responses of the meta turbine designed with different resonator controllers and varying mass ratio between 5% to 20%. (a) TMD resonator, (b) TSD1 resonator, (c) TSD2 resonator, (d) Hybrid-w1w1 resonator, and (e) Hybrid-w1w2 resonator. The liquid assumed is seawater. The amplitude reduction level achieved by controllers attached to the metamaterial turbine is compared in (f).

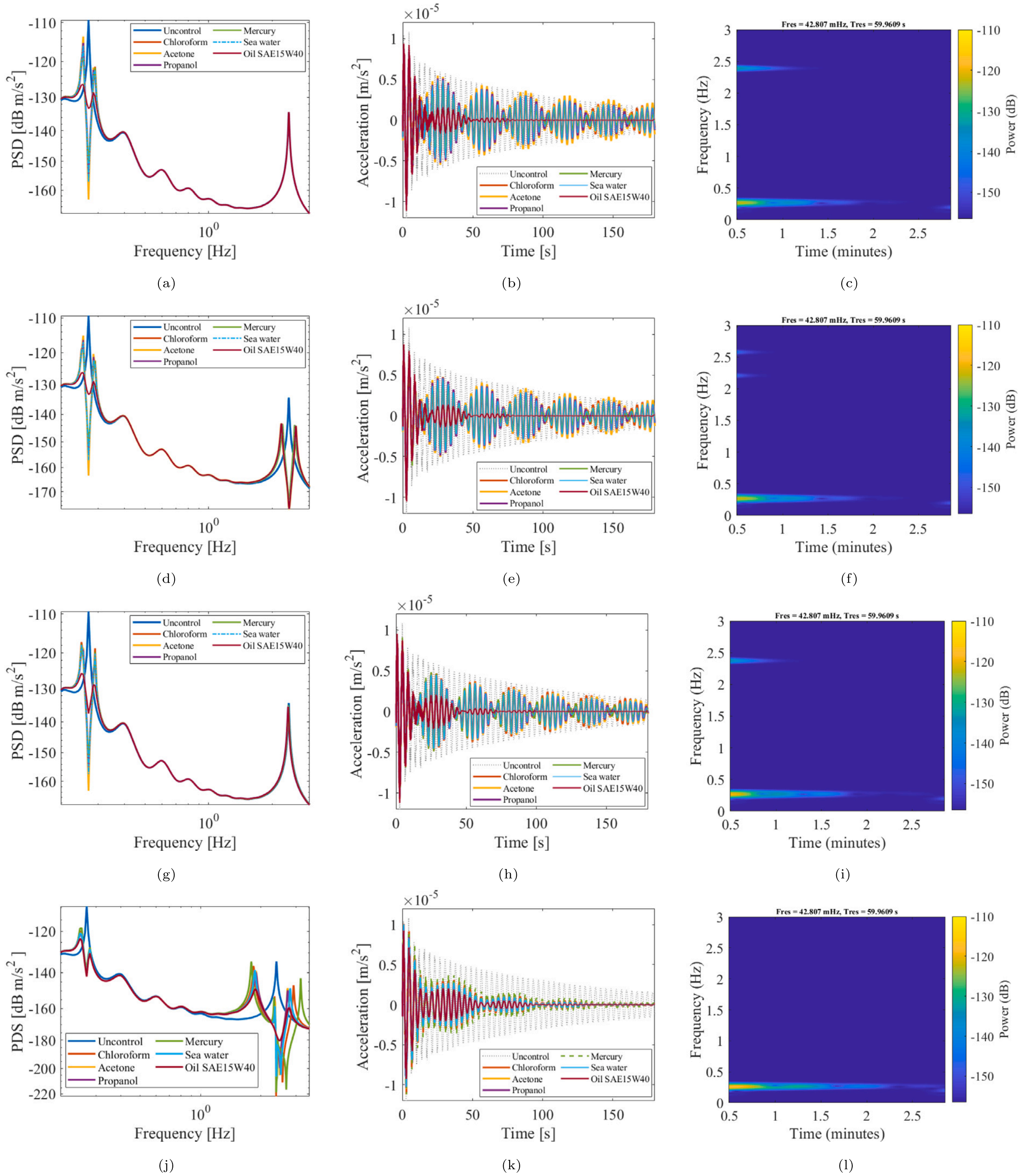

Fig. 15. Auto-spectrum comparing uncontrolled with a controlled turbine for the different liquids in temporal and frequency response, and spectrogram for the best configuration, oil SAE15W40. Metamaterial turbine was designed with ϵ of 10% in the configuration: (a–c) TSD1, (d–f) TSD2, (g–i) Hybrid-w1w1, and (j–l) Hybrid-w1w2.

6. Conclusion

This study presents a new approach to vibration mitigation in offshore wind turbine design based on functional mechanical metamaterial consisting of tuned slosh dampers and hybrid multiphysics resonators. Incorporating the liquid in the dynamic resonators greatly increases the damping factor without adding complexity to the controller devices. The multiphysics metamaterial design combined slosh energy dissipation with oscillating structures to provide additional damping mechanisms, offering a versatile and effective solution for mitigating vibrations in offshore wind turbines under various environmental conditions. Using oil SAE15W40 as the damping liquid was the most effective due to its high viscosity and low density. By modelling the dynamic behaviour of metamaterial OWTs using the DSM and considering multiple hazard excitation forces such as wave, wind, and blade rotation according to international standards (DNV-OS-J101, IEC, and JONSWAP), we have demonstrated the potential of the proposed metamaterial turbine concepts in enhancing vibration control.

Our findings indicate that the designed mechanical metamaterials, which integrate tuned liquid and multiphysics resonators, significantly outperform traditional vibration control methods based on a single TMD and improve the efficiency of TMD metamaterials. The metamaterial turbine solution can achieve scalability and adaptability, improving the resonator controllers' installation, production, and maintenance.

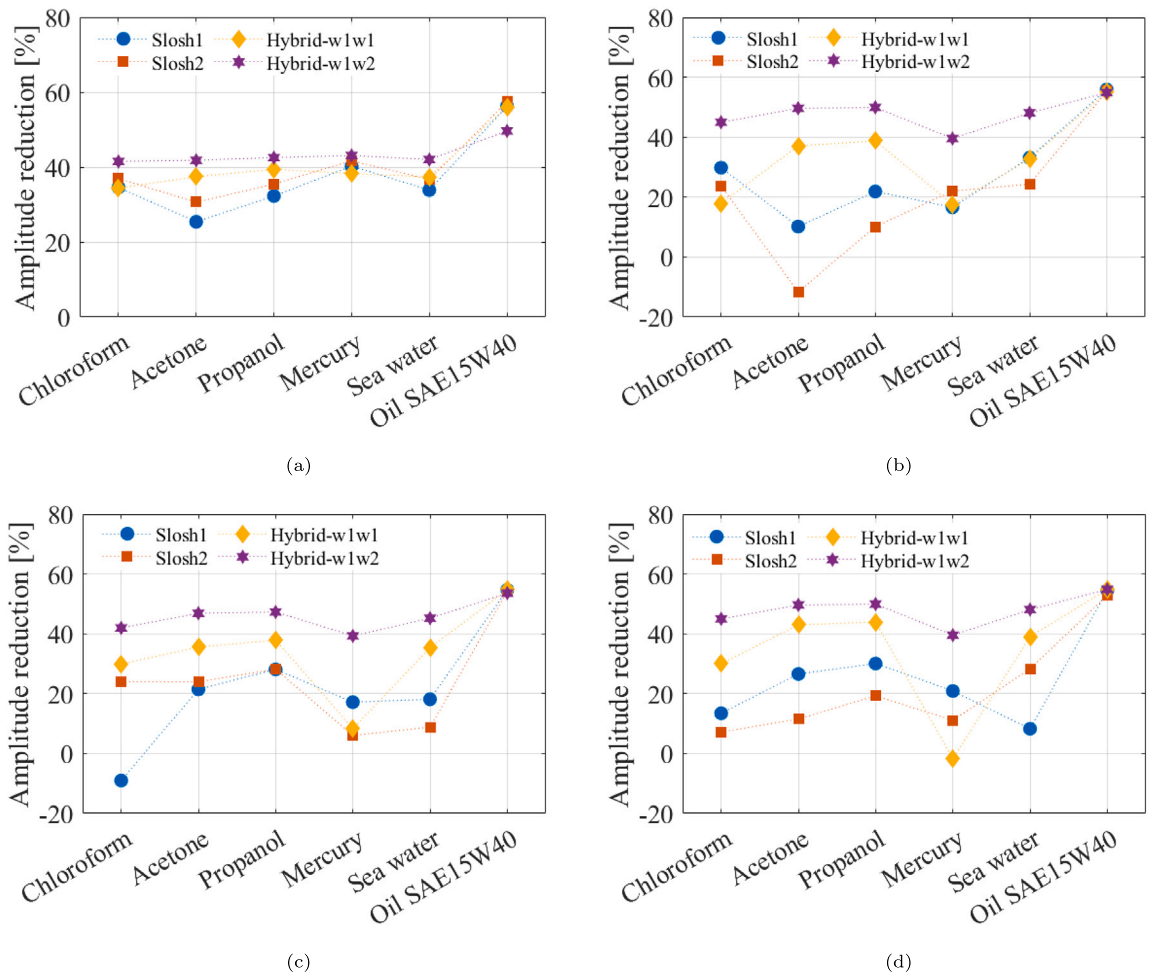

Fig. 16. Amplitude reduction level achieved by controllers TSD and hybrid for different liquids attached to the metamaterial turbine with the mass ratio of (a) 5%, (b) 10%, (c) 15% and (d) 20%.

Compared to traditional methods, the metaturbine significantly reduced vibration amplitudes, achieving a 60% improvement with a small resonator scale versus only 7.8% with conventional TMDs. Overall, the results underline the superiority of multiphysics mechanical metamaterials in vibration control of OWTs, which effectively reduces vibration amplitudes. This innovative approach improves the lifespan, reduces maintenance costs of wind turbines, and provides a robust framework for future advancements in turbine technology. Those functional metamaterials offer a promising solution for improving offshore wind energy systems' structural integrity and operational efficiency, especially in challenging environmental conditions.

CRediT authorship contribution statement

M.R. Machado: Writing – review & editing, Writing – original draft, Software, Project administration, Methodology, Investigation, Funding acquisition, Formal analysis, Conceptualization. **M. Dutkiewicz:** Writing – review & editing, Funding acquisition, Conceptualization.

Declaration of competing interest

The authors declare that they have no known competing financial interests or personal relationships that could have appeared to influence the work reported in this paper.

Acknowledgements

This research is part of the project No. 2022/45/P/ST8/02123 co-funded by the National Science Centre and the European Union Framework Programme for Research and Innovation Horizon 2020 under the Marie Skłodowska-Curie, Poland grant agreement no. 945339.

M.R.M acknowledge the sponsors of projects (CnPQ, Brazil. 404013/2021-0 e 444595/2024-4, Capes, Brazil.88887.975559/2024-00, and FAPDF, Brazil.00193-00002143/2023-02)

Appendix A. Supplementary data

1. Supplementary numerical: Brief description of excitation loads (Wind, Aerodynamic loads of blades during operation, and Wave. Theory of Fig. 13).

2. Supplementary numerical: Validation of the spectral simplified wind turbine.

3 Complementary results: Vibration attenuation with metamaterial OWT under unitary excitation (Figures S3-S6, complement Fig. 9).

4. Complementary results: Enhancing vibration control efficiency with slosh and multiphysics resonators (Figures S7 and S8, complement Fig. 11).

5. Complementary results: Vibration attenuation with metamaterial OWT under multiple hazards excitation forces (Figure S9, complement Fig. 14).

6. Complementary results: Enhancing vibration control efficiency with slosh and multiphysics resonators comparing the various liquids'

performance (Figure S10-S13, complement of Fig. 15).

Supplementary material related to this article can be found online at https://doi.org/10.1016/j.egyr.2025.01.003.

Data availability

Data will be made available on request.

References

Abramson, H., 1966. The Dynamic Behavior of Liquids in Moving Containers, with Applications to Space Vehicle Technology. Tech. Rep., National Aerospace Space Administration (NASA), Special Publication SP-106.

Abramson, H., Chu, W., Jr., R., 1961. Representation of fuel sloshing in cylindrical tanks by an equivalent mechanical model. Am. Rocket. Soc. J. 31 (12), 1697–1705.

Alotta, G., Biondo, C., Giaralis, A., Failla, G., 2023. Seismic protection of land-based wind turbine towers using the tuned inerter damper. Structures 51, 640–656. http://dx.doi.org/10.1016/j.istruc.2023.03.004.

Assouar, M.B., Oudich, M., 2012. Enlargement of a locally resonant sonic band gap by using double-sides stubbed phononic plates. Phys. Rev. Lett. 100, 123506.

Bauer, H., 1962. Theory of Fluid Oscillations in Partially Filled Cylindrical Containers. Tech. Rep., Technical Report MTP-AERO-62-1, NASA-MSFC.

B.Moura, B., Machado, M.R., Mukhopadhyay, T., Dey, S., 2022. Dynamic and wave propagation analysis of periodic smart beams coupled with resonant shunt circuits: Passive property modulation, The European physical. J. Spec. Top. 231.

Brennan, M.J., 2006. Some recent developments in adaptive tuned vibration absorbers/neutralisers. Shock Vib. 13 (4–5), 531–543. http://dx.doi.org/10.1155/2006/563934.

Buckley, T., Watson, P., Cahill, P., Jaksic, V., Pakrashi, V., 2018a. Mitigating the structural vibrations of wind turbines using tuned liquid column damper considering soil-structure interaction. Renew. Energy 120, 322–341. http://dx.doi.org/10.1016/J.RENENE.2017.12.090.

Buckley, T., Watson, P., Cahill, P., Jaksic, V., Pakrashi, V., 2018b. Mitigating the structural vibrations of wind turbines using tuned liquid column damper considering soil-structure interaction. Renew. Energy 120, 322–341. http://dx.doi.org/10.1016/j.renene.2017.12.090.

Burlon, A., Failla, G., 2022. Flexural wave propagation in locally-resonant beams with uncoupled/coupled bending-torsion beam-like resonators. Int. J. Mech. Sci. 215, 106925. http://dx.doi.org/10.1016/j.ijmecsci.2021.106925.

Burton, T., David, S., Jenkins, N., Bossanyi, E., 2001. Wind energy: handbook. J. Wiley.

ling Chen, J., Georgakis, C., 2013. Tuned rolling-ball dampers for vibration control in wind turbines. J. Sound Vib. 332, 5271–5282. http://dx.doi.org/10.1016/J.JSV.2013.05.019.

Chen, J.-L., Georgakis, C.T., 2015. Spherical tuned liquid damper for vibration control in wind turbines. J. Vib. Control 21 (10), 1875–1885. http://dx.doi.org/10.1177/1077546313495911.

ling Chen, J., Georgakis, C., 2015. Spherical tuned liquid damper for vibration control in wind turbines. J. Vib. Control 21, 1875–1885. http://dx.doi.org/10.1177/1077546313495911.

Chen, Y., Jin, X., Liu, H., Li, F., Luo, M., 2021a. Large scale wind turbine TMD optimization based on blade-nacelle-tower-foundation coupled model. Ocean Eng. 239, 109764. http://dx.doi.org/10.1016/j.oceaneng.2021.109764.

Chen, Y., Jin, X., Luo, M., Cheng, P., Wang, S., 2021b. Vibration reduction methods of large-scale wind turbines based on system-TMD coupled algorithm. Ocean Eng. 226, http://dx.doi.org/10.1016/j.oceaneng.2021.108832.

Chen, J., Zhan, G., Zhao, Y., 2016. Application of spherical tuned liquid damper in vibration control of wind turbine due to earthquake excitations. Struct. Des. Tall Spec. Build. 25 (10), 431–443. http://dx.doi.org/10.1002/tal.1266.

Chen, J.-l., Zhao, Y., Cong, O., He, M.-j., 2018. Vibration control using double-response damper and site measurements on wind turbine. Struct. Control Health Monit. 25 (9), http://dx.doi.org/10.1002/stc.2200.

Colherinhas, G.B., Girao de Morais, M.V., Machado, M.R., 2022. Spectral model of offshore wind turbines and vibration control by pendulum tuned mass dampers. Int. J. Struct. Stab. Dyn. 22 (05), http://dx.doi.org/10.1142/S0219455422500535.

Colwell, S., Basu, B., 2009. Tuned liquid column dampers in offshore wind turbines for structural control. Eng. Struct. 31 (2), 358–368. http://dx.doi.org/10.1016/j.engstruct.2008.09.001.

Dalela, S., Balaji, P.S., Jena, D.P., 2022. A review on application of mechanical metamaterials for vibration control. Mech. Adv. Mater. Struct. 29 (22), 3237–3262. http://dx.doi.org/10.1080/15376494.2021.1892244.

deMoura, B., Machado, M., Dey, S., Mukhopadhyay, T., 2024. Manipulating flexural waves to enhance the broadband vibration mitigation through inducing programmed disorder on smart rainbow metamaterials. Appl. Math. Model. 125, 650–671. http://dx.doi.org/10.1016/j.apm.2023.10.011.

Det Norske Veritas, A.S., 2014. Design of Offshore Wind Turbine Structures. DNV-OS-J101 - Offshore Standard.

Dezvareh, R., Bargi, K., Mousavi, S.A., 2016. Control of wind/wave-induced vibrations of jacket-type offshore wind turbines through tuned liquid column gas dampers. Struct. Infrastruct. Eng. 12 (3), 312–326. http://dx.doi.org/10.1080/15732479.2015.1011169.

Ding, H., Chen, Y.-N., Wang, J.-T., Altay, O., 2022. Numerical analysis of passive toroidal tuned liquid column dampers for the vibration control of monopile wind turbines using FVM and FEM. Ocean Eng. 247, http://dx.doi.org/10.1016/j.oceaneng.2022.110637.

Doyle, J.F., 1997. Wave Propagation in Structures : Spectral Analysis Using Fast Discrete Fourier Transforms, second ed. In: Mechanical engineering, Springer-Verlag New York, Inc., New York.

El-Borgi, S., Fernandes, R., Rajendran, P., Yazbecka, R., Boyd, J.G., Lagoudas, D.C., 2020. Multiple bandgap formation in a locally resonant linear metamaterial beam: Theory and experiments. J. Sound Vib. 488, 115647.

Fath, A., Azadi Yazdi, E., Eghtesad, M., 2020. Semi-active vibration control of a semi-submersible offshore wind turbine using a tuned liquid multi-column damper. J. Ocean Eng. Mar. Energy 6 (3), 243–262. http://dx.doi.org/10.1007/s40722-020-00171-x.

Francesco, R.A., Felice, A., Giuseppe, F., 2024. Water-tank metabarrier for seismic Rayleigh wave attenuation. Phil. Trans. R. Soc. A 38220230363. http://dx.doi.org/10.1098/rsta.2023.0363.

Fu, L., Guo, T., Li, G., 2018. Investigation on damping performance of new type oscillator-liquid combined damper. Int. J. Mech. Sci. 135, 53–62. http://dx.doi.org/10.1016/j.ijmecsci.2017.11.018.

Ghaemmaghami, A.R., Kianoush, R., Mercan, O., 2016. Numerical modeling of dynamic behavior of annular tuned liquid dampers for the application in wind towers under seismic loading. J. Vib. Control 22 (18), 3858–3876. http://dx.doi.org/10.1177/1077546314567524.

Ghaemmaghami, A., Kianoush, R., Yuan, X.-X., 2013. Numerical modeling of dynamic behavior of annular tuned liquid dampers for applications in wind towers. Computer- AIDED Civ. Infrastruct. Eng. 28 (1), 38–51. http://dx.doi.org/10.1111/j.1467-8667.2012.00772.x.

Ghassempour, M., Failla, G., Arena, F., 2019. Vibration mitigation in offshore wind turbines via tuned mass damper. Eng. Struct. 183, 610–636. http://dx.doi.org/10.1016/j.engstruct.2018.12.092.

He, E.-M., Hu, Y.-Q., Zhang, Y., 2017. Optimization design of tuned mass damper for vibration suppression of a barge-type offshore floating wind turbine. J. Eng. Marit. Enviroment 231 (1), 302–315. http://dx.doi.org/10.1177/1475090216642466.

Hemmati, A., Oterkus, E., Khorasanchi, M., 2019. Vibration suppression of offshore wind turbine foundations using tuned liquid column dampers and tuned mass dampers. Ocean Eng. 172, 286–295. http://dx.doi.org/10.1016/j.oceaneng.2018.11.055.

Hu, Y., Wang, J., Chen, M.Z.Q., Li, Z., Sun, Y., 2018. Load mitigation for a barge-type floating offshore wind turbine via inerter-based passive structural control. Eng. Struct. 177, 198–209.

Hussein, M.I., Leamy, M.J., Ruzzene, M., 2014. Dynamics of phononic materials and structures: Historical origins, recent progress, and future outlook. Appl. Mech. Rev. 66 (4), http://dx.doi.org/10.1115/1.4026911.

Ibrahim, R.A., 2005. Liquid Sloshing Dynamics: Theory and Applications. Cambridge University Press.

IEC, 2005. Wind turbines - Part 1: Design Requirements. International Electrotechnical Commission (IEC) 61400-1, International Standard.

Jahangiri, V., Sun, C., 2022. A novel three dimensional nonlinear tuned mass damper and its application in floating offshore wind turbines. Ocean Eng. 250, 110703. http://dx.doi.org/10.1016/j.oceaneng.2022.110703.

Jahangiri, V., Sun, C., Kong, F., 2021. Study on a 3D pounding pendulum TMD for mitigating bi-directional vibration of offshore wind turbines. Eng. Struct. 241, http://dx.doi.org/10.1016/j.engstruct.2021.112383.

Jonkman, J.M., Butterfield, S., Musial, W., Scott, G., 2009. Definition of a 5-MW Reference Wind Turbine for Offshore System Development [Electronic Resource]. National Renewable Energy Laboratory, p. x, 63, URL https://www.nrel.gov/docs/fy09osti/38060.pdf.

Jonkman, J.M., Musial, W., 2010. Offshore Code Comparison Collaboration (OC3) for IEA Task 23 Offshore Wind Technology and Deployment [Electronic Resource]. National Renewable Energy Laboratory, p. v, 70, URL https://www.nrel.gov/docs/fy11osti/48191.pdf.

Karimi, H.R., Zapateiro, M., Luo, N., 2010. Semiactive vibration control of offshore wind turbine towers with tuned liquid column dampers using Hinfty output feedback control. In: 2010 IEEE International Conference on Control Applications. pp. 2245–2249. http://dx.doi.org/10.1109/CCA.2010.5611186.

Konar, T., Ghosh, A.D., 2021. Adaptation of a deep liquid-containing tank into an effective structural vibration control device by a submerged cylindrical pendulum appendage. Int. J. Struct. Stab. Dyn. 21 (06), 2150078. http://dx.doi.org/10.1142/S0219455421500784.

Konar, T., Ghosh, A.D., 2023a. Development and design of a deep tank damper with submerged suspended plate. Adv. Struct. Eng. 26 (5), 937–951. http://dx.doi.org/10.1177/13694332221145341.

Konar, T., Ghosh, A.D., 2023b. A review on various configurations of the passive tuned liquid damper. J. Vib. Control 29 (9–10), 1945–1980. http://dx.doi.org/10.1177/10775463221074077.

Lee, U., 2009. Spectral Element Method in Structural Dynamics. John Wiley & Sons, (Asia) Pte Ltd, http://dx.doi.org/10.1002/9780470823767.

Lei, M., Xu, L., Huang, J., 2023. Spatiotemporal multiphysics metamaterials with continuously adjustable functions. Mater. Today Phys. 34, 101057. http://dx.doi.org/10.1016/j.mtphys.2023.101057.

Li, C., Zhuang, T., Zhou, S., Xiao, Y., Hu, G., 2017. Passive vibration control of a semi-submersible floating offshore wind turbine. Appl. Sci.- Basel 7 (6), http://dx.doi.org/10.3390/app7060509.

Liao, M., Wu, Y., 2021. Conceptual design and dynamic analysis of a novel passive floating offshore wind turbine structure. Ships Offshore Struct. 16 (10), 1040–1049. http://dx.doi.org/10.1080/17445302.2020.1791684.

Liu, Z., Wang, Y., Hua, X., Zhu, H., Zhu, Z., 2021a. Optimization of wind turbine TMD under real wind distribution countering wake effects using GPU acceleration and machine learning technologies. J. Wind Eng. Ind. Aerodyn. 208, http://dx.doi.org/10.1016/j.jweia.2020.104436.

Liu, Z., Wang, Y., Nyangi, P., Zhu, Z., Hua, X., 2021b. Proposal of a novel GPU-accelerated lifetime optimization method for onshore wind turbine dampers under real wind distribution. Renew. Energy 168, 516–543. http://dx.doi.org/10.1016/j.renene.2020.12.073.

Liu, Z., Zhang, X., Mao, Y., Zhu, Y., Yang, Z., Chan, C., Sheng, P., 2000. Locally resonant sonic materials science. Science 289, 1734–1736. http://dx.doi.org/10.1126/science.289.5485.1734.

Machado, M., Dos Santos, J., 2021. Effect and identification of parametric distributed uncertainties in longitudinal wave propagation. Appl. Math. Model. 98, 498–517. http://dx.doi.org/10.1016/j.apm.2021.05.018.

Machado, M.R., Dutkiewicz, M., 2024a. Enhancing broadband vibration suppression of a cable conductor using graded metamaterials. J. Braz. Soc. Mech. Sci. Eng. 46 (190), 1806–3691. http://dx.doi.org/10.1007/s40430-024-04722-3.

Machado, M., Dutkiewicz, M., 2024b. Wind turbine vibration management: An integrated analysis of existing solutions, products, and open-source developments. Energy Rep. 11, 3756–3791. http://dx.doi.org/10.1016/j.egyr.2024.03.014.

Machado, M., Dutkiewicz, M., Colherinhas, G., 2024. Metamaterial-based vibration control for offshore wind turbines operating under multiple hazard excitation forces. Renew. Energy 223, 120056. http://dx.doi.org/10.1016/j.renene.2024.120056.

Machado, M.R., Moura, B., Dey, S., Mukhopadhyay, T., 2022. Bandgap manipulation of single and multi-frequency smart metastructures with random impedance disorder. Smart Mater. Struct. 31.

McNamara, K.P., Love, J.S., Tait, M.J., Haskett, T.C., 2021. Response of an annular tuned liquid damper equipped with damping screens. J. Vib. Acoust. - Trans. ASME 143 (1), http://dx.doi.org/10.1115/1.4047863.

Munson, R., Young, D., Okiishi, T., 1995. Fundamentals of Fluid Mechanics. John Wiley & Sons, USA.

Ocak, A., Bekdaş, G., Nigdeli, S.M., Kim, S., Geem, Z.W., 2022. Optimization of tuned liquid damper including different liquids for lateral displacement control of single and multi-story structures. Buildings 12 (3), http://dx.doi.org/10.3390/buildings12030377.

Roberts, P., Chen, J., Basurto, E., 1966. Slosh Design Handbook. Tech. Rep., I - NASA-CR-406, NASA.

Sardar, R., Chakraborty, S., 2022. Wave vibration control of jacket platform by tuned liquid dampers. Ocean Eng. 247, http://dx.doi.org/10.1016/j.oceaneng.2022.110721.

Sarkar, S., Chakraborty, A., 2019. Development of semi-active vibration control strategy for horizontal axis wind turbine tower using multiple magneto-rheological tuned liquid column dampers. J. Sound Vib. 457, 15–36. http://dx.doi.org/10.1016/j.jsv.2019.05.052.

Sharma, V., Arun, C., Krishna, I.P., 2019. Development and validation of a simple two degree of freedom model for predicting maximum fundamental sloshing mode wave height in a cylindrical tank. J. Sound Vib. 461, 114906. http://dx.doi.org/10.1016/j.jsv.2019.114906.

Singleton, L., Cheer, J., Daley, S., 2019. Design of a resonator-based metamaterial for broadband control of transverse cable vibration. In: Ochman, M. (Ed.), Proceedings of the 23rd International Congress on Acoustics. Deutsche Gesellschaft für Akustik e.V. (DEGA), pp. 5589–5596, URL https://eprints.soton.ac.uk/434378/.

Sinha, P., Mukhopadhyay, T., 2023. Programmable multi-physical mechanics of mechanical metamaterials. Mater. Sci. Eng. 155, 100745. http://dx.doi.org/10.1016/j.mser.2023.100745.

Stedman, T., Woods, L., 2017. Cloaking of thermoelectric transport. Sci. Rep. 7, 6988. http://dx.doi.org/10.1038/s41598-017-05593-6.

Sugino, C., Leadenham, S., Ruzzene, M., Erturk, A., 2016. On the mechanism of bandgap formation in locally resonant finite elastic metamaterials. J. Appl. Phys. 120–13, 4963648.

Sun, C., Jahangiri, V., 2018. Bi-directional vibration control of offshore wind turbines using a 3D pendulum tuned mass damper. Mech. Syst. Signal Process. 105, 338–360. http://dx.doi.org/10.1016/j.ymssp.2017.12.011.

Tsao, W.-H., Chen, Y.-C., Kees, C.E., Manuel, L., 2023. Response mitigation of floating platform by porous-media-tuned liquid dampers. J. Offshore Mech. Artic Eng. - ASME 145 (5), http://dx.doi.org/10.1115/1.4062292.

Verma, M., Nartu, M.K., Subbulakshmi, A., 2022. Optimal TMD design for floating offshore wind turbines considering model uncertainties and physical constraints. Ocean Eng. 243, http://dx.doi.org/10.1016/j.oceaneng.2021.110236.

Villoslada, D., Santos, M., Tomas-Rodriguez, M., 2022. TMD stroke limiting influence on barge-type floating wind turbines. Ocean Eng. 248, http://dx.doi.org/10.1016/j.oceaneng.2022.110781.

Wang, G., Wen, X., Wen, J., Shao, L., Liu, Y., 2004. Two-dimensional locally resonant phononic crystals with binary structures. Phys. Rev. Lett. 93, 154302.

Wu, L., Li, Y., 2021. Harnessing bulging or sloshing modes to design locally resonant liquid-solid metamaterials. J. Sound Vib. 510, 116280. http://dx.doi.org/10.1016/J.JSV.2021.116280.

Xiao, Y., Wen, J., Yu, D., Wen, X., 2013. Flexural wave propagation in beams with periodically attached vibration absorbers: Band-gap behavior and band formation mechanisms. J. Sound Vib. 332 (4), 867–893. http://dx.doi.org/10.1016/j.jsv.2012.09.035.

Xie, F., Aly, A.-M., 2020. Structural control and vibration issues in wind turbines: A review. Eng. Struct. 210, 110087. http://dx.doi.org/10.1016/j.engstruct.2019.110087.

Xu, X., Chen, Y., Zhang, S., Song, J., Huang, G., 2019. Experimental demonstration of a dissipative multi-resonator metamaterial for broadband elastic wave attenuation. Science 438, 1–12. http://dx.doi.org/10.1126/science.289.5485.1734.

Xu, X., Guo, T., Li, G., Sun, G., Shang, B., Guan, Z., 2018. A combined system of tuned immersion mass and sloshing liquid for vibration suppression: Optimization and characterization. J. Fluids Struct. 76, 396–410. http://dx.doi.org/10.1016/j.jfluidstructs.2017.10.011.

Xu, L., Wang, J., Dai, G., Yang, S., Yang, F., Wang, G., Huang, J., 2021. Geometric phase, effective conductivity enhancement, and invisibility cloak in thermal convection-conduction. Int. J. Heat Mass Transfer 165, 120659. http://dx.doi.org/10.1016/j.ijheatmasstransfer.2020.120659.

Xue, M.-A., Dou, P., Zheng, J., Lin, P., Yuan, X., 2022. Pitch motion reduction of semisubmersible floating offshore wind turbine substructure using a tuned liquid multicolumn damper. Mar. Struct. 84, http://dx.doi.org/10.1016/j.marstruc.2022.103237.

Yang, T., Bai, X., Gao, D., Wu, L., Li, B., Thong, J.T.L., Qiu, C.-W., 2015. Invisible sensors: Simultaneous sensing and camouflaging in multiphysical fields. Adv. Mater. 27 (47), 7752–7758. http://dx.doi.org/10.1002/adma.201502513.

Yang, Y., Bashir, M., Li, C., Michailides, C., Wang, J., 2020. Mitigation of coupled wind-wave-earthquake responses of a 10 MW fixed-bottom offshore wind turbine. Renew. Energy 157, 1171–1184. http://dx.doi.org/10.1016/j.renene.2020.05.077.

Yang, J., He, E.M., Hu, Y.Q., 2019. Dynamic modeling and vibration suppression for an offshore wind turbine with a tuned mass damper in floating platform. Appl. Ocean Res. 83, 21–29. http://dx.doi.org/10.1016/j.apor.2018.08.021.

Zhang, Z., Basu, B., Nielsen, S.R.K., 2019a. Real-time hybrid aeroelastic simulation of wind turbines with various types of full-scale Tuned Liquid Dampers. Wind Energy 22 (2), 239–256. http://dx.doi.org/10.1002/we.2281.

Zhang, C., Cao, W.K., Yang, J., Ke, J.C., Chen, M.Z., Wu, L.T., Cheng, Q., Cui, T.J., 2019b. Multiphysical digital coding metamaterials for independent control of broadband electromagnetic and acoustic waves with a large variety of functions. ACS Appl. Mater. Interfaces 11 (18), 17050–17055. http://dx.doi.org/10.1021/acsami.9b02490.

Zhang, Z., Hoeg, C., 2018. Vibration control of floating offshore wind turbines using liquid column dampers. In: Science of Making Torque from Wind (TORQUE 2018). In: Journal of Physics Conference Series, vol. 1037, Politecnico Milano, Dept Aerosp Sci & Technol, http://dx.doi.org/10.1088/1742-6596/1037/3/032002, 7th Conference on Science of Making Torque from Wind (TORQUE), Milan, ITALY, JUN 20-22, 2018.

Zhang, Z., Hoeg, C., 2020. Dynamics and control of spar-type floating offshore wind turbines with tuned liquid column dampers. Struct. Control Health Monit. 27 (6), http://dx.doi.org/10.1002/stc.2532.

Zhang, Z., Hoeg, C., 2021. Inerter-enhanced tuned mass damper for vibration damping of floating offshore wind turbines. Ocean Eng. 223, 108663.

Zhang, Z., Nielsen, S., Basu, B., Li, J., 2015. Nonlinear modeling of Tuned Liquid Dampers (TLDs) in rotating wind turbine blades for damping edgewise vibrations. J. Fluids Struct. 59, 252–269. http://dx.doi.org/10.1016/J.JFLUIDSTRUCTS.2015.09.006.

Zhang, Z., Staino, A., Basu, B., Nielsen, S., 2016. Performance evaluation of full-scale Tuned Liquid Dampers (TLDs) for vibration control of large wind turbines using real-time hybrid testing. Eng. Struct. 126, 417–431. http://dx.doi.org/10.1016/J.ENGSTRUCT.2016.07.008.

Zhang, T., Wang, W., Li, X., Wang, B., 2023. Vibration mitigation in offshore wind turbine under combined wind-wave-earthquake loads using the tuned mass damper inerter. Renew. Energy 216, 119050.

Zhang, Q., Zhang, K., Hu, G., 2018. Tunable fluid-solid metamaterials for manipulation of elastic wave propagation in broad frequency range. Appl. Phys. Lett. http://dx.doi.org/10.1063/1.5023307.

Zhang, Y., Zhao, X., Wei, X., 2020. Robust structural control of an underactuated floating wind turbine. Wind Energy 23 (12), 2166–2185. http://dx.doi.org/10.1002/we.2550.

Zhong, R., Pai, P.F., Zong, Z., Deng, H., Ruan, X., 2018. Metamaterial I-Girder for vibration absorption of composite cable-stayed bridge. J. Eng. Mech. 144 (7), 04018045. http://dx.doi.org/10.1061/(ASCE)EM.1943-7889.0001467.

Zhou, W., Wu, B., Su, Y., Liu, D., Chen, W., Bao, R., 2021. Tunable flexural wave band gaps in a prestressed elastic beam with periodic smart resonators. Mech. Adv. Mater. Struct. 28 (3), 221–228. http://dx.doi.org/10.1080/15376494.2018.1553261.

Zuo, H., Bi, K., Hong, H., 2020. Simultaneous out-of-plane and in-plane vibration mitigations of offshore monopile wind turbines by tuned mass dampers. Smart Struct. Syst. 26 (4), 435–449. http://dx.doi.org/10.12989/sss.2020.26.4.435.